EVALUATION OF FIELD QUANTITIES AT THE SURFACE OF A CORONATING MONOPOLAR SINGLE CONDUCTOR USING THE FINITE ELEMENT METHOD

by

MATHUR KRISHNA VENKATESHA

A thesis
presented to the University of Manitoba
in partial fulfillment of the
requirements for the degree of
Master of Science
in
Electrical Engineering

Winnipeg, Manitoba

ISBN 0-315-34041-X

EVALUATION OF FIELD QUANTITIES AT THE SURFACE OF A CORONATING MONOPOLAR SINGLE CONDUCTOR USING THE FINITE ELEMENT METHOD

BY

MATHUR KRISHNA VENKATESHA

A thesis submitted to the Faculty of Graduate Studies of the University of Manitoba in partial fulfillment of the requirements of the degree of

MASTER OF SCIENCE

I hereby declare that I am the sole author of this thesis.

I authorize the University of Manitoba to lend this thesis to other institutions or individuals for the purpose of scholarly research.

M. K. Venkatesha

I further authorize the University of Manitoba to reproduce this thesis by photocopying or by other means, in total or in part, at the request of other institutions or individuals for the purpose of scholarly research.

M. K. Venkatesha

The University of Manitoba requires the signatures of all persons using or photocopying this thesis. Please sign below, and give address and date.

ABSTRACT

In this thesis an algorithm is presented for the evaluation of the field quantities at the surface of a monopolar coronating conductor. The basic goal of this work is to determine, numerically, the variation and magnitude of the electric field intensity around the surface of the coronating conductor. A finite element based scheme has been used to solve the ionized field problem. The algorithm has been implemented for conductors of both positive and negative polarity. In the proposed scheme the third boundary condition required to obtain a solution to the ionized field problem is supplied in the form of measured ionic current density distribution at ground level.

The results show that, following the onset, the average conductor gradient drops below Peek's onset value. The extent of this drop is shown to depend on the applied voltage. It is also shown that the electric field at the surface of a coronating conductor varies around its periphery. The extent of variation is greater than that before onset.

ACKNOWLEDGEMENTS

The author wishes to express his sincere thanks to his supervisors Dr. M. R. Raghuveer and Dr. I. R. Ciric for their patient supervision, guidance and invaluable suggestions throughout the course of this work.

On a personal note, gratitudes are due to author's parents,grand parents, sister and Professor K.A. Krishnamurthy for their encouragement and understanding over the years.

This thesis is dedicated to my late grand mother.

CONTENTS

LIST OF FIGURES

LIST OF TABLES

Chapter I

INTRODUCTION

One of the important factors which affects the design of a HVDC transmission line is its corona performance. Corona is an electric field related phenomenon which occurs when the electric field at the surface of a conductor exceeds a critical value known as the onset gradient[14]. Consider the case of a single conductor situated at a constant height above a perfectly conducting ground. If the voltage applied to the conductor is increased, the associated electric field also increases in direct proportion. The field is Laplacian and remains so until the electric gradient at the surface of the energized conductor exceeds the onset gradient. At this point, the surrounding air gets ionized; i.e. the air may no longer be considered as a perfect dielectric. In fact due to ionization, ions exist in the space between the conductor and ground. It is the movement of these ions that constitutes corona current and the associated power loss.

HVDC transmission line corona is an extremely complex phenomenon. It depends on design factors such as applied voltage, line geometry and other parameters such as conductor surface irregularities, weather conditions(relative humidity,rain,fog,snow etc.) and atmospheric purity(dust content).

The phenomenon of corona on overhead HVDC transmission lines manifests itself as a steady unidirectional flow of ionic species, away from the electrode in corona. In the case of unipolar corona, the polarity of the ionic species coincides with that of the coronating electrode. In bipolar corona, ions of each polarity are generated near the corresponding pole of the HVDC line. Positive ions dominate the region between the positive pole and ground, while negative ions take up the corresponding space near the opposite pole. In the zone between the two poles, ionic species of both polarities are present.

The occurrence of corona generates audible noise, radio and TV interference; besides as already mentioned, it causes power loss[11]. Also, the generated ions cause the electric field at ground level to increase beyond the electrostatic value. The ions close to the coronating conductor have velocities far in excess of normal wind velocities. However, as the ions move away from the energized conductor their velocities decline and, in the low field areas, become comparable to typical wind velocities. Under such conditions the movement of ions can be influenced by wind[21]. Consequently it is possible for ions generated by a transmission line to accumulate on metallic or dielectric objects situated downwind and remote from the line. This process results in the charging up of the objects and thus constitutes a shock hazard[20]. There is also considerable concern regarding

the biological effects of the ionic current. All the above mentioned effects are of practical importance because the present day practice is to design transmission lines which operate at voltage levels well beyond onset. For example, the conductors of the Nelson river transmission line are scheduled to operate at a theoretical gradient of 25 kV/cm. Taking into account a surface factor of 0.5[21], the effective gradient is approximately 50 kV/cm and the line will be operating well into corona. It should be clear from the above that the predetermination of the corona performance of a line is important.

1.1 Problem formulation

For all cases of DC corona, the flow of ions is determined by the magnitude and direction of the local electric field intensity E. This quantity in turn, is the result of, on the one hand, the effects of electrode geometry and on the other the influences of all charges distributed in space. As a consequence, the electric field intensity vector is governed by both, the potentials applied to the electrodes, and the space charge distribution which is influenced by the electric field E. This mutual interaction between the fundamental quantities is reflected in the mathematical formulation where the permittivity of free space, ϵ, and ion mobility k are also taken into account.

The system of equations describing the monopolar corona discharge in the steady state are

$$\nabla . \nabla \Phi = -\rho/\epsilon \tag{1.1}$$

$$\nabla . (\rho \nabla \Phi) = 0 \tag{1.2}$$

These equations represent the Poisson's equation and the inhomogeneous Laplace's equation respectively. The electric field as derived from the scalar potential Φ is

$$E = -\nabla \Phi \tag{1.3}$$

In equation (1.2) ρ, volume charge density, is a function of position. The simultaneous solution of Φ and ρ from equations (1.1) and (1.2) yields the solution to the corona problem.

Equations (1.1) and (1.2) can be represented by a single third order, nonlinear partial differential equation, namely

$$\nabla . ((\nabla . \nabla \Phi) \nabla \Phi) = 0 \tag{1.4}$$

This is the general form of equation describing monopolar corona.

Solution of the DC ionized field is in general, extremely difficult because of the nonlinearity of the equations describing it. Furthermore, the main difficulty in the theoretical analysis is that, at the conductor surface no elec-

trical quantities except its potential are known. Thus all attempts in the literature are based on some simplifying assumptions.

1.2 Boundary conditions

The following boundary conditions are used in the analysis of the problem.

The potential on the coronating conductor is known.

$$\Phi = V \tag{1.5}$$

The potential on the ground plane is zero.

$$\Phi = 0 \tag{1.6}$$

Since for transmission line configurations, the domain is unbounded, an artificial boundary is placed at a suitable distance from the energized conductor, with the potential on that boundary assumed to be equal to the corresponding electrostatic value

$$\Phi = \Phi_{es}$$

The two boundary conditions equations (1.5) and (1.6) are not sufficient to obtain a unique solution to the problem. Therefore, the first attempts at a solution were based on the Deutsch assumption which states that the presence of the

space charge affects only the magnitude and not the direction of the electric field. The assumption simplifies the problem because it reduces 2-dimensional ionized field problems to a 1-dimensional problem. However, the methods employing Deutsch's assumption yield accurate results at low levels of corona current only[11].

Deutsch's assumption has been waived by many researchers who adopted a finite element technique to solve the ionized field problem. However, a third boundary condition is still necessary. To fulfill this condition the researchers have used the Kaptzov assumption which states that after onset of corona the magnitude of the electric field intensity on the conductor surface remains constant at its onset value, regardless of the magnitude of the applied voltage.

Yet another group of researchers [17] have provided the third boundary condition in the form of constant charge density of the corresponding polarity on the surface of each source conductor. The drawback of their method is that ρ, the charge density is not known a priori. In order to arrive at a solution the authors use experimentally determined values of total current emitted by a full scale model of the transmission line. The authors, however do not present any results concerning the variation of field quantities around the coronating conductor surface.

The invalidity of the Kaptzov's assumption is easily ascertained from physical considerations[10]. Consider a monopolar transmission line with the conductor energized at positive polarity, at a voltage greater than the onset value. In this case the electrons are attracted towards the conductor. In the high field areas they are effective ionizers and positive ions are produced. The fast moving electrons are neutralized at the anode leaving behind a cloud of slow moving positive ions which effectively lower the electric field at the conductor surface. The percent decrease in the surface electric field depends on the positive ion charge density and will not be the same at all points on the conductor periphery. The situation about a negative charged monopolar conductor is different. Here, the electrons are repelled from the conductor and form avalanches in the high field region. The electrons move quickly away from the corroding conductor leaving behind a cloud of positive ions which journey slowly towards the conductor where, eventually, they get neutralized. However the presence of the ionic space charge increases the electric field at the conductor surface. As in the previous case the percent increase is not uniform at all points on the circumference but depends on the space charge density.

Experimental evidence provided by Popkov [15] supports the conclusions arrived at above from consideration of the basic physical process. Popkov's investigation of fields at

the conductor surface was carried out by using an incandescent probe. His experimental line consisted of a conductor of radius 0.056 cm which was held at a constant height of 25 cm above a ground plane. Measurements were carried out at both positive and negative polarities to yield the distribution of ion density, potential and electric field E. Popkov concluded that there is a variation in the electric field around the conductor surface; the extent of variation was found to depend on the charge density.

1.3 Thesis objective

The main objective of this thesis is to determine, numerically, the nature of the variation and magnitude of the electric field around the surface of a coronating monopolar conductor; i.e. to examine the validity of Kaptzov's assumption. A finite element based technique has been used to solve equations (1.1) and (1.2) iteratively and calculations have been performed for both positively and negatively charged conductor. As explained earlier a third boundary condition is necessary to enable a solution of the ionized field problem. In the present work this is supplied in the form of known values of ionic current density at the ground as determined experimentally. Using this value, an algorithm has been developed which enables the determination of all the field quantities at the surface of the coronating conductor.

Three geometries have been examined in this thesis; in each case, for the voltage levels considered, accurate values of ionic current density at ground level measured under still air conditions were available from literature.

Before a finite element solution could be implemented it was found necessary to examine certain aspects concerning the accuracy of the electrostatic field solution and its dependance on mesh size, growth, shape and nature of the interpolating polynomial. This work is presented in chapter II.

Chapter III deals with the solution of the ionized field. The field quantities at the conductor surface have been computed. Chapter IV presents the conclusions of this work.

Chapter II

ELECTROSTATIC FIELD SOLUTION OF A MONOPOLAR DC TRANSMISSION LINE

The electrostatic field solution under HVDC lines obtained by application of the finite element method, FEM, is important not only by itself but also because it may be used to evaluate the accuracy of the FEM solution of the associated ionized field. Indeed, the solution of the ionized field problem employs the same Laplacian operator; the accuracy of this solution which is obtained on an iterative basis can not be checked because an exact analytical solution does not exist. The determination of the accuracy of the Finite Element electrostatic solution for the monopolar single conductor geometry, on the other hand, is possible because of the existence of an exact method for the calculation of the electrostatic field.

Another important reason for considering the analysis of the electrostatic field is that the algorithm set up in this thesis(Chapter 3) for the calculation of the electric field at the surface of the coronating conductor employs, initially, the electrostatic value. Naturally it is desirable to use accurate values. Also, the potential at nodes on the artificial boundary is maintained at its electrostatic value. It is therefore obvious that the electrostatic analysis

is very important. Furthermore, it is known that the accuracy of a finite element solution is dependent on the type of the mesh, mesh density and growth[3]. Since the same mesh has been used for the ionized field solution, the accuracy of the electrostatic solution will provide some information regarding the accuracy of the ionized field results obtainable from that mesh.

The accuracy of the FEM electrostatic solution was assessed by performing computations on two models of a transmission line of the general geometry shown in Figure 2.1 which also shows the values of the H and r in the two models.

Due to the large H/r ratio, typical of transmission lines, the choice of element shape, density and growth pattern becomes critical especially in the high field region. The choice of the interpolating polynomial is also important and is related to mesh density.

Two different meshes were used in the analysis. For model 1, a mesh composed of 195 principle nodes and 335 elements was used with 15 conductor nodes and 14 ground nodes. For model 2 the mesh consisted of 121 principle nodes , 195 elements, 11 conductor nodes and 10 ground nodes. This finite element mesh is shown in Figure 2.2 which also shows the artificial boundary. It may be noted that that the artificial boundary meets the ground at a lateral distance of 6.3H where H is the conductor height. The bipolar system of

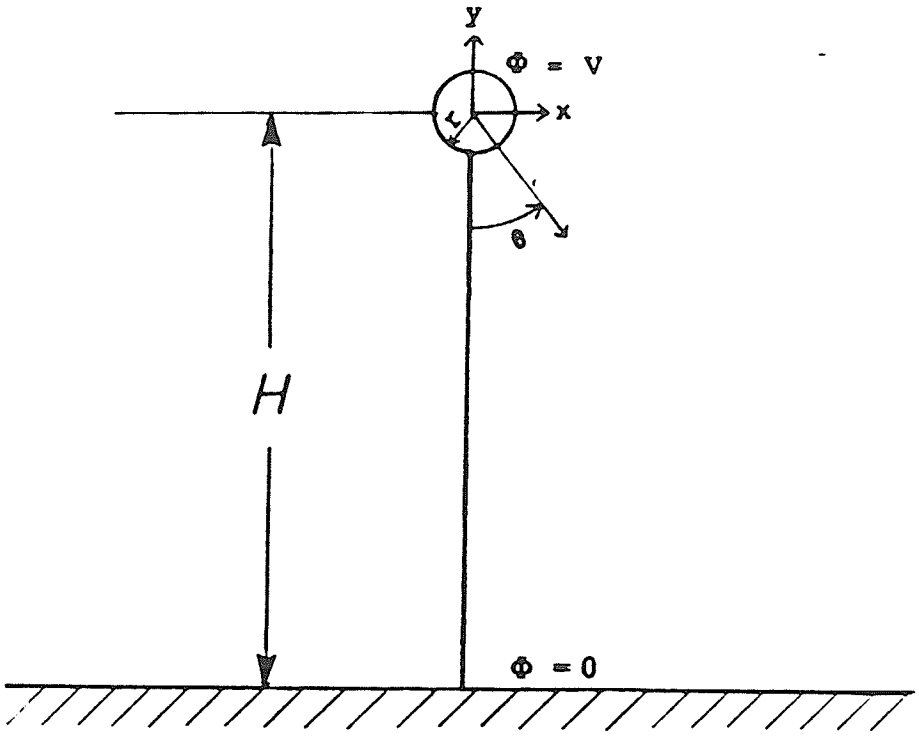

Figure 2.1 Conductor to plane geometry

	model 1	model 2
H (cm)	200.0	40.0
r (cm)	0.25	0.165
H/r	800	242

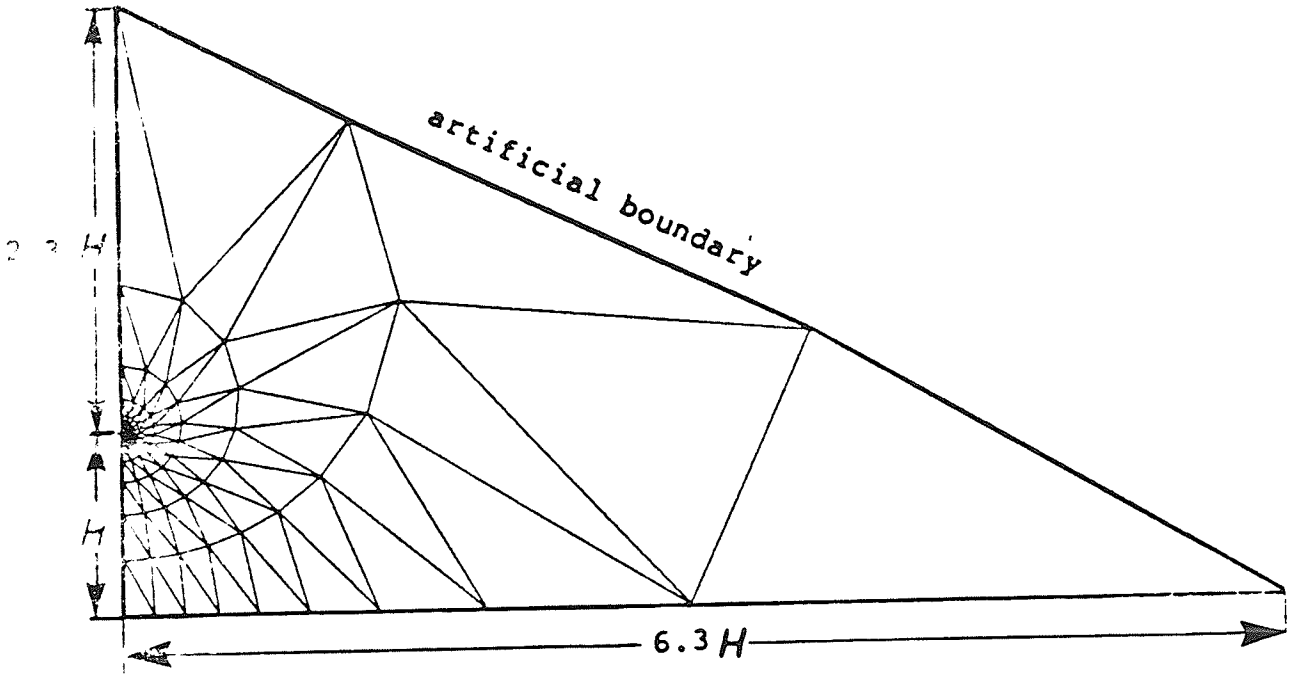

Figure 2.2 Finite Element Mesh of model 2

coordinates (Chapter 3) was employed to fix the location of the nodes, the basis for which will be made clear in the next chapter.

Dirichlet conditions were enforced on the conductor and ground. The potential at nodes on the artificial boundary was calculated by replacing the conductor with a filamentary line charge at its geometrical center and imaging it with respect the ground plane. For the chosen configuration, the expression for potential at any point (x,y) is given by

$$\Phi = A \ ln \frac{(x^2 + (y + 2H)^2)}{(x^2 + y^2)} \qquad (2.1)$$

and the electric field is evaluated using its component values,

$$E_x = \frac{-8AHx(H + y)}{(x^2 + y^2)(x^2 + (y + 2H)^2)} \qquad (2.2)$$

$$E_y = \frac{4AH(y^2 + 2Hy - x^2)}{(x^2 + y^2)(x^2 + (y^2 + 2H)^2)} \qquad (2.3)$$

In equations (2.1)-(2.3) A is a constant and can be found by enforcing the Dirichlet condition in equation (2.1). For large H/r values i.e. H/r > 100, equations (2.1)-(2.3) may be considered to yield almost exact values[21].

The accuracy of the electrostatic solution was assessed by comparing the numerical results with those obtained from equations (2.1)-(2.3). This comparison was carried out at

nodes on the ground, the conductor surface and along the vertical line joining the center of the conductor to ground.

Initial computations were carried out using linear, quadratic and cubic elements; the accuracy of the results obtained using these interpolating polynomials were compared[18] with each other. The comparison study indicated that best results are obtained with the use of quadratic elements. An advantage of employing quadratic elements is that the conductor surface can be modelled faithfully, using isoparametric elements.

Since a node is shared by more than one element, there are as many values for E as there are elements which share that node. In order to obtain a unique value for E, an averaging process has to be resorted to. For example, one may compute the arithmetic mean or the area weighted mean value or the value obtained from centroidal length weighting; i.e.

$$E_{node} = \frac{\sum_{i=1}^{6} E_i}{n} \qquad \text{arithmetic mean weighted average}$$

$$E_{node} = \frac{\sum_{i=1}^{6} A_i E_i}{\sum_{i=1}^{n} A_i} \qquad \text{area weighted average} \qquad (2.4)$$

$$E_{node} = \frac{\sum_{i=1}^{6} l_i E_i}{\sum_{i=1}^{n} l_i} \qquad \text{centroidal length weighted average}$$

where

n = number of elements which share a common node

E_i = electric field of the i^{th} element

A_i = area of the i^{th} element

A comparison study indicated[18] that, except on the conductor surface, there is not much difference in the values of E obtained by employing the three averaging methods. On the conductor surface, the use of the area weighting technique provides only a slightly better result. Based on these findings, it was decided to use quadratic interpolating polynomials and calculate the electric field at a node by computing the arithmetic mean of the field values contributed by all elements sharing that node.

2.1 Discussion of results

The results obtained from the electrostatic analysis of monopolar single conductor geometry, for both models are presented in Tables 2.1-2.6. The conductors of models 1 and 2 were assigned potentials of 300 and 80 kV respectively. The variation of electrostatic potential and field along the vertical line joining the center of the conductor to ground is shown in Table 2.1 for model 1 and Table 2.4 for model 2. Tables 2.2 and 2.5 present information regarding the variation of the electrostatic field intensity around the conductor surface for the two models. Field variations along the ground are shown in Tables 2.3 and 2.6 for models 1 and 2

respectively. From these Tables it is seen that all errors, in both field and potential, are less than 1%. Tables 2.1 and 2.4 show that for both models, the error in potential is maximum at a node next to the ground node on the vertical line joining the center of the conductor to ground. The maximum error in the electric field, however, does not occur at this node, but at a location much closer to the conductor. Comparison of the data in Tables 2.2,2.3,2.5 and 2.6 shows that the maximum error in $|E|$ along the vertical line joining the conductor center to ground is greater than the errors around the conductor and along the ground.

It may be noted that, along the ground the maximum error in $|E|$ occurs at a lateral distance in excess of four times the conductor height in both models. The magnitude of the error is less than 1%. Errors in the angle of E were also monitored. They were found to be much lower than errors in the corresponding magnitudes of E. Figures 2.3 and 2.4 show the variation of the electrostatic field around the conductor surface. In model 1 the variation, defined by:

$$[\text{Max. } |E| - \text{Min. } |E|]/\text{Max. } |E|$$

is 0.133%. The corresponding value for model 2 is 0.363%. The reason for the large variation in the latter case is due to reduced value of the ratio H/r.

From the above, it is concluded that the use of quadratic elements and the arithmetic mean averaging technique of electric field calculation results in extremely good accura-

cy for the finite element electrostatic solution of the geometry of models 1 and 2. Since the same mesh is used to obtain the ionized field solution, one expects that the mesh characteristics and the finite element field calculation techniques adopted will contribute insignificantly to the overall error.

A brief discussion of the finite element method and its implementation is included in Appendix A.

r (cm)	Exact potential (kV)	Computed potential (kV)	%Error	Exact E field kV/cm	Computed E field kV/cm	%Error
0.25	300.00	300.00	0.000	162.77	162.64	0.086
0.46	274.96	275.13	0.050	88.105	88.018	0.099
0.85	250.01	250.13	0.048	47.754	47.583	0.358
1.58	225.01	225.11	0.042	25.920	25.790	0.498
2.90	200.01	200.18	0.082	14.110	14.030	0.595
5.34	175.01	175.15	0.080	7.724	7.669	0.712
9.76	150.01	150.10	0.062	4.272	4.245	0.632
17.7	125.01	125.12	0.089	2.407	0.389	0.748
31.5	100.01	100.09	0.086	1.401	1.393	0.571
54.6	75.01	75.11	0.137	0.862	0.858	0.464
90.5	50.00	50.13	0.244	0.581	0.577	0.688
140.4	25.00	25.08	0.316	0.446	0.443	0.673
200.0	0.00	0.00	-	0.407	0.4064	0.067

Table 2.1 Variation of Φ and E along the line $\theta = 0$

(model 1, Φ = 300 kV)

θ^0	Exact E field kV/cm	Computed E field kV/cm	% Error
0.0	162.766	162.626	0.086
12.847	162.762	162.476	0.175
25.663	162.757	162.346	0.253
38.509	162.745	162.322	0.259
51.365	162.727	162.309	0.257
64.204	162.712	162.301	0.253
77.059	162.688	162.292	0.243
90.000	162.664	162.284	0.234
102.74	162.641	162.277	0.224
115.62	162.623	162.268	0.218
128.47	162.601	162.260	0.209
141.38	162.591	162.257	0.205
154.24	162.571	162.246	0.200
167.12	162.563	162.239	0.199
180.00	162.55	162.228	0.198

Table 2.2 Variation of E around the conductor (model 1, Φ = 300 kV)

x m	Exact *E* field kV/cm	Computed *E* field kV/cm	% Error
0.000	406.662	406.389	0.067
0.225	401.564	401.236	0.082
0.457	386.526	386.189	0.087
0.699	362.302	362.127	0.048
0.963	380.106	329.863	0.074
1.257	291.553	291.243	0.106
1.595	248.577	248.391	0.075
1.999	203.332	203.284	0.024
2.508	158.086	158.009	0.049
3.183	115.109	115.046	0.064
4.153	76.558	76.436	0.158
5.176	44.361	44.281	0.179
8.760	20.136	20.098	0.191

Table 2.3 Variation of *E* along ground

(model 1, Φ= 300 kV)

y cm	Exact potential kV	Computed potential kV	%Error	Exact E field kV/cm	Computed E field kV/cm	%Error
0.165	80.000	80.000	0.000	78.590	78.486	0.132
0.305	72.001	72.047	0.065	42.536	42.448	0.207
0.565	64.013	64.043	0.047	23.081	22.997	0.364
1.041	56.004	56.032	0.050	12.591	12.509	0.651
1.911	48.003	48.028	0.052	6.937	6.879	0.836
3.476	40.002	40.024	0.055	3.892	3.856	0.925
6.219	32.010	32.019	0.028	2.256	2.249	0.310
10.822	24.007	24.014	0.029	1.383	1.377	0.434
18.000	16.004	16.011	0.044	0.927	0.924	0.324
28.012	8.001	8.021	0.249	0.711	0.708	0.429
40.000	0.000	0.000	-	0.647	0.6468	0.568

Table 2.4 Variation of Φ and E along the line $\theta = 0$

(model 2, $\Phi = 80$ kV)

θ^0	Exact E field kV/cm	Computed E field kV/cm	%Error
0.0	78.590	78.486	0.132
17.93	78.582	78.441	0.179
35.86	78.561	78.424	0.174
53.79	78.527	78.403	0.158
71.72	78.482	78.384	0.125
89.65	78.432	78.318	0.145
107.58	78.385	78.271	0.145
125.51	78.344	78.239	0.134
143.44	78.311	78.207	0.133
161.37	78.298	78.204	0.120
180.00	78.288	78.201	0.111

Table 2.5 Variation of E around the conductor (model 2, Φ= 80 kV)

x cm	Exact *E* field kV/cm	Computed *E* field kV/cm	%Error
0.00	647.064	646.873	0.187
6.34	631.209	630.982	0.359
12.99	585.276	585.109	0.285
20.38	513.701	513.584	0.228
29.06	423.512	423.396	0.274
40.00	323.535	323.469	0.204
55.06	223.559	223.491	0.304
78.50	133.367	133.286	0.607
121.11	61.791	61.736	0.890
252.55	15.835	15.826	0.568

Table 2.6 Variation of *E* along ground (model 2, Φ = 80 kV)

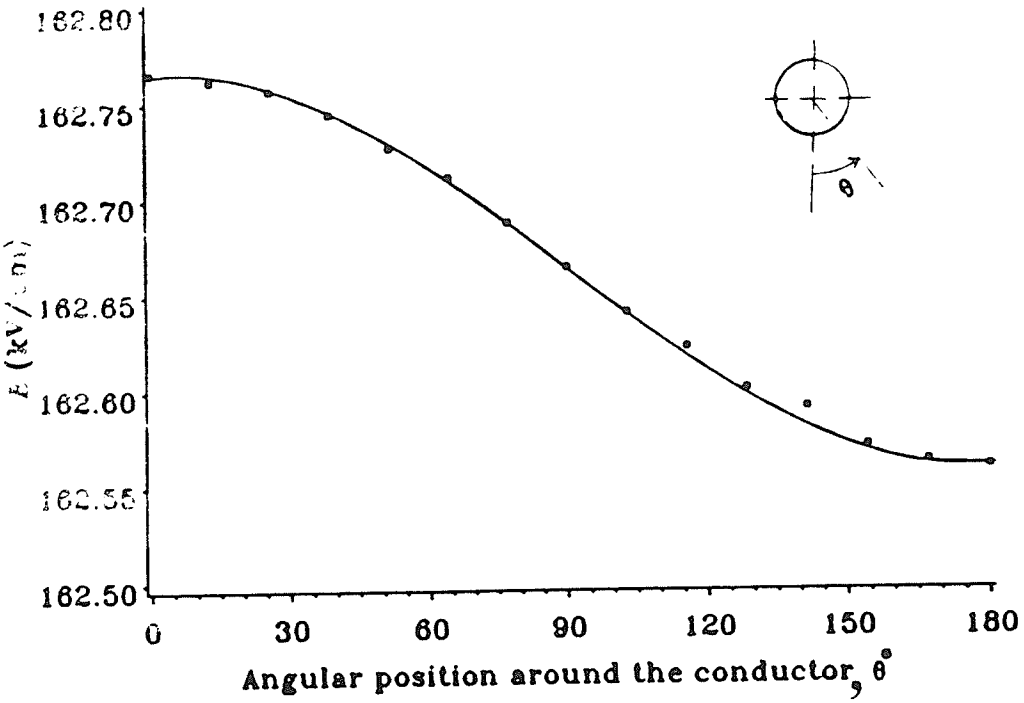

Figure 2.3 Variation of E around the conductor surface for model 1 at Φ=300 kV

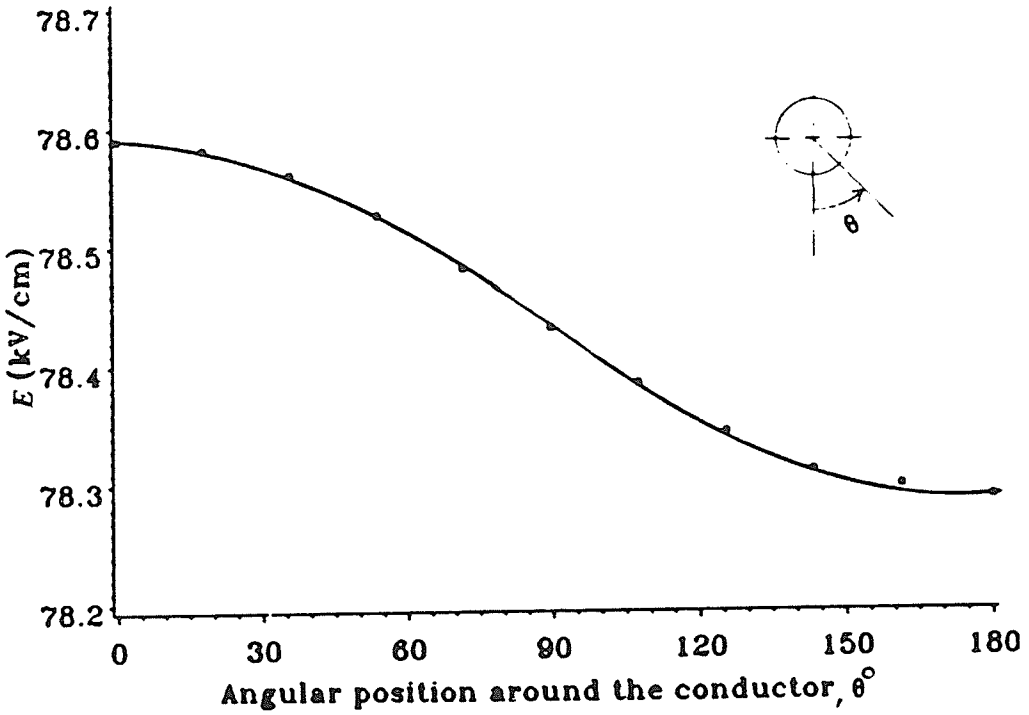

Figure 2.4 Variation of E around the conductor surface for model 2 at Φ =80 kV

Chapter III

ANALYSIS OF DC IONIZED FIELD

As pointed out earlier, the basic goal of this thesis is is to evaluate the magnitude and variation of the field quantities E and ρ around the surface of a coronating monopolar conductor and to examine the dependence of these quantities on conductor potential. Such an analysis requires, that the conductor field gradient, for potentials greater than the onset value, is not constant at the onset value i.e. the Kaptzov assumption can not be utilized. Therefore the third boundary condition is supplied in the form of experimental values of current density at ground level. These experimental values will have to be obtained under still air condition as the analysis does not take into account wind effects. No measurements were conducted in this work; the experimental values were obtained from literature. The analysis has been carried out for three different models, some characterstics of which are included in Table 3.1. Figure 3.1 shows the experimentally obtained current density distribution at ground level for each of the models.

For the sake of completeness, the equations governing monopolar corona are described below.

	Model 1	Model 2	Model 3
Reference #	[8]	[2]	[15]
Author	M. Hara et. al	Abdel Salam	V.I. Popkov
H	200 cm	40 cm	25 cm
r	0.25 cm	0.165 cm	0.056 cm
H/r	800	242	446
Data available	J,*E*	J	J,I
Φ	200V,300 kV	80 kV	50 kV
Onset voltage	93.8kV	56.55 kV	27.75 kV
+ve onset gradient	50.84kV/cm	55.42kV/cm	72.92kV/cm
- ve onset gradient	52.92kV/cm		

Table 3.1 Some features of the models under consideration

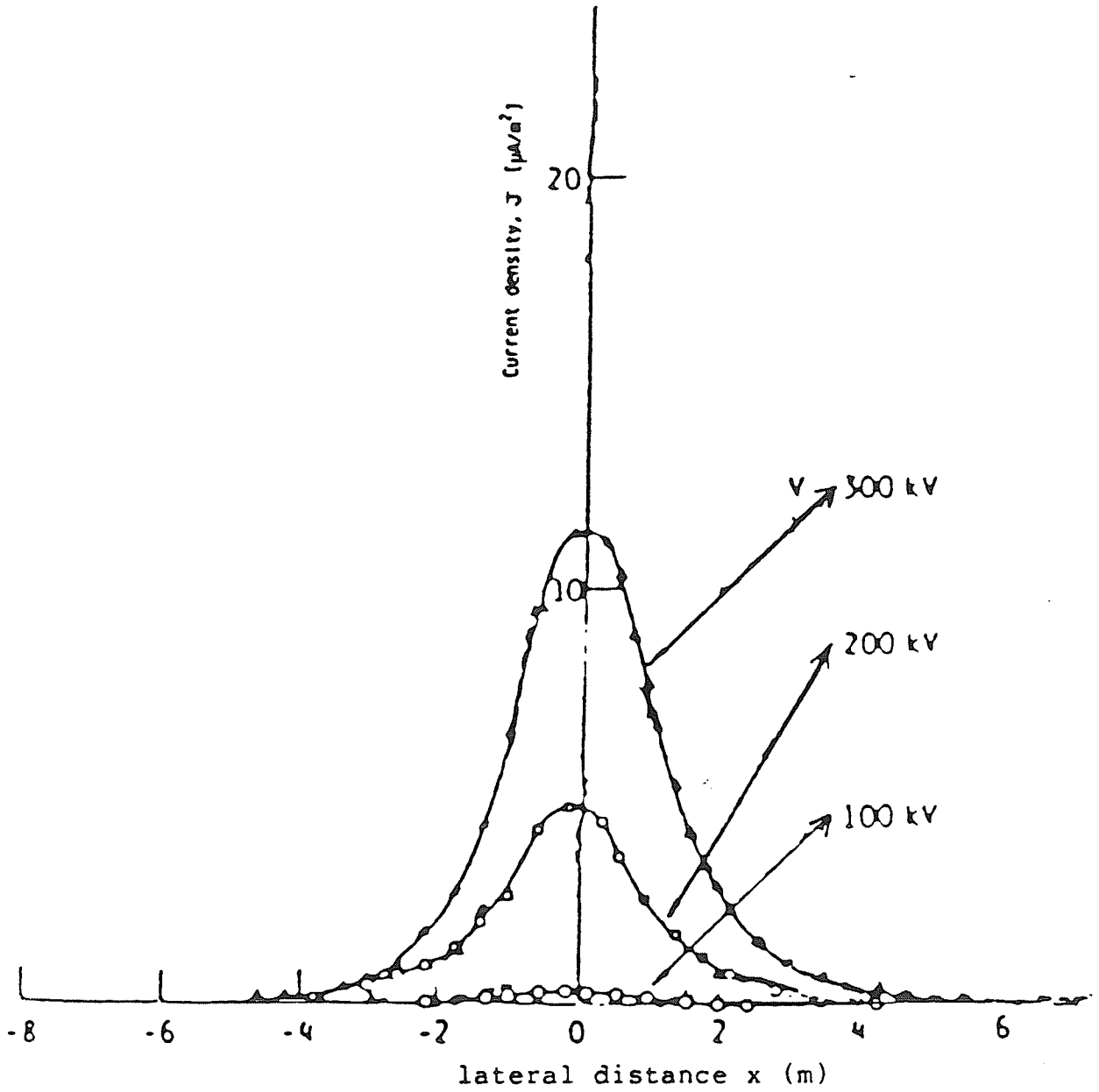

Figure 3.1.1 Measured ionic current density distribution for model 1 obtained from [8]

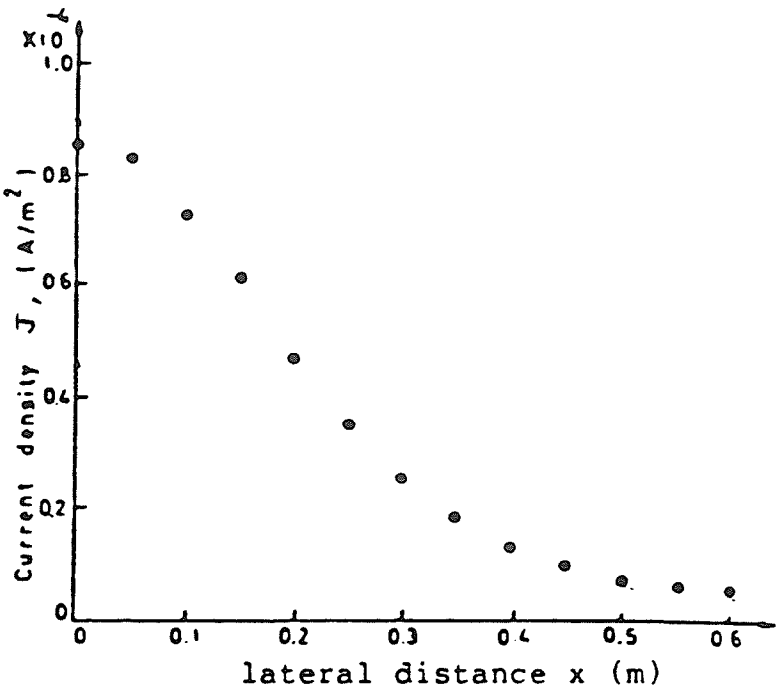

Figure 3.1.2 Measured ionic current density distribution for model 2 obtained from [2]

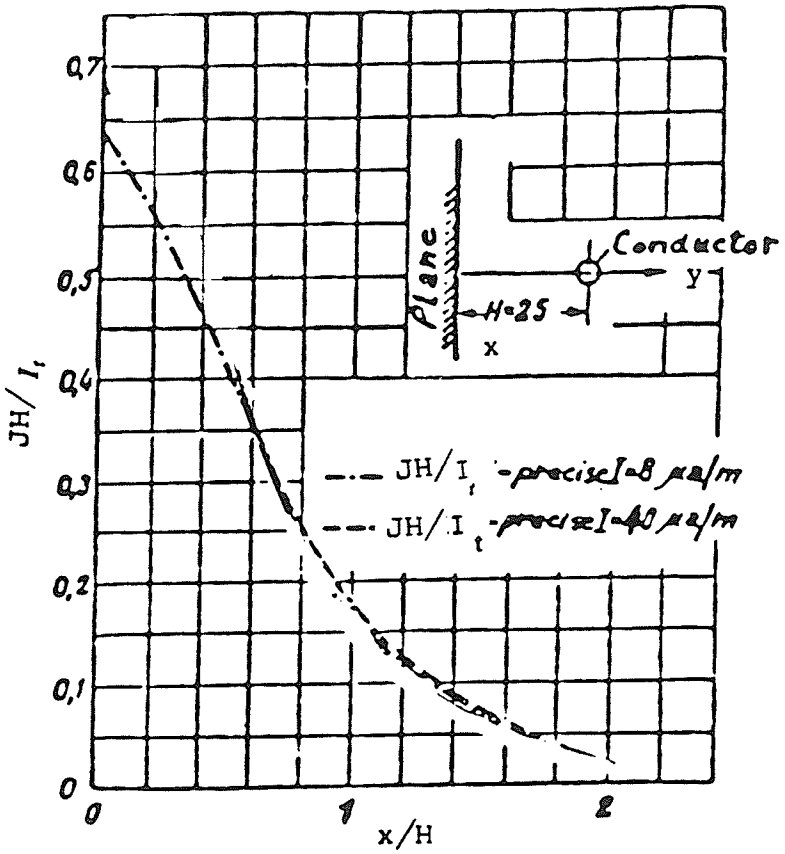

Figure 3.1.3 Ionic current density distribution for model 3 obtained from [15].

I_t is the total corona current.

3.1 Mathematical model of monopolar corona

The system of equations describing the monopolar corona discharge in the steady state are

$$\nabla . \nabla \Phi = - \rho/\epsilon \qquad (3.1)$$

$$\nabla . (\rho \nabla \Phi) = 0 \qquad (3.2)$$

The electric field as derived from the scalar potential is

$$E = - \nabla \Phi \qquad (3.3)$$

The above system of equations (3.1)-(3.2) can be replaced by a single third order, nonlinear partial differential equation namely,

$$\nabla . ((\nabla . \nabla \Phi) \nabla \Phi) = 0 \qquad (3.4)$$

Equation (3.4) requires three boundary conditions for its solution. However, only two are available in the form of conductor potential and ground potential. The selection of the third boundary condition plays an important role in the solution of equations (3.1)-(3.2). Besides, no information is available regarding the distribution of E, Φ and ρ in the interelectrode space.

An analytical treatment yielding closed-form expressions is possible only in a few simple cases which exhibit high

symmetry i.e. infinite parallel plates, infinitely long coaxial cylinders and concentric spheres. In such cases equation (3.4) reduces to an ordinary differential equation.

As an example consider the geometry of an infinitely long coaxial cylinder shown in Figure 3.2. The inner conductor is held at a potential V while the outer one is grounded. Symmetry dictates that all electrical quantities viz. ϕ, E and ρ are functions of radial position r in cylindrical coordinates. The governing equations in cylindrical coordinates are

$$(1/r)\ d/dr\,(r\,d\Phi/dr) = -\rho/\epsilon \tag{3.5}$$

$$1/r\ d/dr\ (r\rho\, d\Phi/dr) = 0 \tag{3.6}$$

From equation (3.6),

$$r\ \rho\, d\Phi/dr = K$$

$$-r_1\,\rho_e\,E_o = K \tag{3.7}$$

From equation (3.7),

$$r\ d\Phi/dr = -r_1\,\rho_e\,E_o/\rho$$

From equation (3.5),

$$(1/r)\ d/dr\,(r_1\,\rho_e\,E_o/\rho) = \rho/\epsilon$$

$$(E_o\,\rho_e\,r_1)/r\ \ d/dr\,(1/\rho) = \rho/\epsilon$$

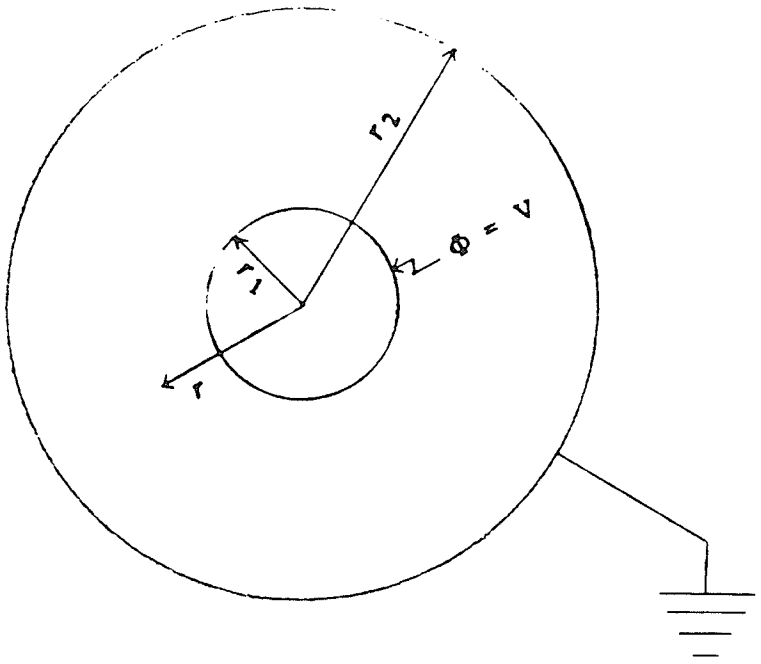

Figure 3.2 Coaxial cylindrical geometry.

$$(-E_o\ \rho_e\ r_1/r)\ (1/\rho^2)\ d\rho/dr = \rho/\epsilon$$

$$-d(\rho/\rho^3) = r\ dr/(\epsilon\ E_o\ \rho_e\ r_1)$$

$$(1/2)\ (1/\rho^2) = r^2/(2\epsilon_o\ E_o\ \rho_e\ r_1)$$

$$1/\rho^2 = 1/\rho_e^2 + (r^2-r_1^2)/\epsilon_o\ E_o\ \rho_e\ r_1$$

$$\rho = \sqrt{\left(\frac{\epsilon_o\ E_o\ \rho_e\ r_1}{(r^2-r_1^2)+\epsilon_o\ E_o\ r_1/\rho_e}\right)} \qquad (3.8)$$

$$d\Phi/dr = (k_1/r)\ \sqrt{r^2+p^2}$$

where

$$k_1 = \sqrt{(r_1\ \rho_e\ E_o/\epsilon)}$$

and $p^2 = \epsilon\ E_o\ r_1/\rho_e - r_1^2$

$$\Phi(r) = -k_1[\sqrt{(r^2+p^2)} - p\ ln(p+\sqrt{(r^2+p^2)}/r)]\ B$$

Imposing the boundary condition at $r=r_1$ we obtain,

$$\Phi(r) = V - k_1[f_1(r) - k_2 + k_3(ln(r/r_1) + ln(k_3+k_2) - ln(k_3+f(r)))] \qquad (3.9)$$

where

$$k_2 = k_1\epsilon/\rho_e$$

$$k_3 = \sqrt{(r_1\ E_o\ \epsilon\ \rho_e)}/f_1(r)$$

$$f_1(r) = \sqrt{(r^2-r_1^2+k_2^2)}$$

From the foregoing analysis, it is evident that it is very difficult to obtain a closed form solution of the ionized field problem. It can also be noted that one has to solve the transcendental equation (3.9) to obtain the value of ρ_e. Knowing ρ_e, the value of E and all other field quantities at any radial distance can be found. Two other simple cases which can be dealt with in similar fashion are geometries of the infinite parallel plate and concentric spherical configurations. All other cases must rely on some simplifying assumptions and numerical formulations.

3.2 Steps involved in the ionized field solution of monopolar corona

A logical iterative scheme using a numerical method (FEM) consists of the following steps.

Step 1: Discretize the problem domain into finite elements.

Step 2: Specify initial values of ρ in the problem domain at all nodes.

Step 3: Solve equation (3.1) for potential, with the values of ρ chosen as in step 2 and compute E and J values at all nodes. The mobility, k^+ or k^-, depending on the polarity of the energized conductor, is assumed to be constant.

Step 4: Using the same values of ρ used in step 2, solve equation (3.2) for potential and compute the field quantities E and J at all nodes in the problem domain.

Step 5: The field solution obtained in steps 3 and 4 will differ if the distribution of ρ is incorrect. i.e. the potential and field values at any node obtained in steps 3 and 4 will differ. Therefore, in step 5, the value of ρ is corrected so as to bring the potential and field values computed from equations (3.1)-(3.2) as close to each other as possible at all nodes. This is accomplished by using the most recent field values from steps 3 and 4 in an updating formula for the charge density.

Step 6: Steps 3-5 are repeated until specified convergence criterion are met.

Each of the above steps is discussed below in detail.

Step 1; construction of the Finite Element mesh

Table 3.2 summarizes the characterstics of the meshes used to obtain the ionized field solution of models 1 - 3.

In all cases a quadratic interpolating polynomial was used. The electric field was calculated using the arithmetic mean technique as explained in chapter II. In the case of model 3 with an H/r ratio of 446, as shown in Table 3.1, the mesh is identical to the one used for analyzing model 2. As already mentioned, the solution of the differential equations governing corona, using FEM, requires the problem domain to be subdivided into small elements. In this work the location of the nodes is chosen so as to reproduce the bipolar coordinate system (ξ,η).

	Model 1	Model 2	Model 3
Reference#	[8]	[2]	[15]
H/r	800	242	446
Number of nodes	195(727)	121(440)	121(440)
Number of elements	335	195	195
Number of ground nodes	14	10	10
Number of conductor nodes	15	11	11
Lateral distance of the farthest ground node from the conductor center	8.75H	6.3H	6.3H

Table 3.2 Characterstics of the meshes used in the analysis.

While the nodes are defined and identified by their cartesian coordinates(x,y), the numerical values for the latter are selected in such a way so as to satisfy the conditions

$$\xi = Constant$$

$$\eta = Constant$$

The relations between the two sets of coordinates, cartesian(x,y) and bipolar (ξ,η) are

$$x = C\frac{\sin \eta}{(\cosh \xi + \cos \eta)}$$

$$y = C\frac{\sinh \xi}{(\cosh \xi + \cos \eta)}$$

where

$C = \sqrt{H^2 - r^2}$ and

H is the height of the conductor above ground and r is the conductor radius.

If ξ is kept constant, the locus of points plotted in cartesian coordinates, traces out a circle. The center of the circle is located on the y axis at the point (0,C cothξ) and its radius is C coshξ .

Similarly if ξ is allowed to vary, keeping η constant, the circles are centered at (-C cotη ,0.0) with a radius of C cosecη .

As ξ and η are independent of each other and since the constant ξ and η circles are centered along the x and y axes respectively, the two families of circles are mutually orthogonal to each other at the point of intersection. In-

deed, for the geometry considered i.e. cylindrical conductor at constant height above a plane, the constant ξ circles define equipotential lines and constant η circles define the flux lines in the absence of corona. Choice of the node placement as described above proves to be advantageous while executing the numerical procedure.

The finite element mesh was generated by using a semiautomatic procedure, the program for implementation of which is shown in Appendix C.

3.2.2 Step 2; selection of initial ρ distribution

The initial values of ρ at all nodes were specified as follows. First the total current emitted by the conductor at a particular voltage was computed by finding the area enclosed by the ground ionic current density profiles(i.e. Figure 3.1.1 for model 1). Alternatively, this current may be obtained directly from the VI characterstic if available.

Next, since the corona current density around the conductor surface is known to be cosinusoidal, [13] the conductor current density value at any angular position, θ, J was written as,

$$J(\theta) = J_{max.} \cos\left(\frac{\theta}{2}\right) \qquad (3.10)$$

where

$$J_{max.} = J(\theta=0) = J_b$$

The total corona current, I_t, is calculated by integrating J around the conductor surface.

$$I_t = 2r \int_0^{\pi} J(\theta) d(\theta) \qquad (3.11)$$

which yields

$$J_b = \frac{I_t}{4r}$$

The charge density values at conductor nodes was calculated using the relation

$$J = k \rho E_{es} \qquad (3.12)$$

where

J=J(θ) and

$k = k^+$ or k^- depending on the conductor polarity and

E_{es} = electrostatic field quantity at that node.

As mentioned earlier, the finite element nodes are located using the bipolar coordinate system. Consider the set of nodes A,...,J which are located at the intersection of the circle $\eta = \eta_3$ and the circles $\xi = \xi_1, \ldots \xi = \xi_{10}$. as in Figure 3.3. These nodes lie on an electrostatic flux line AJ.

In order to find the initial value of ρ at nodes such as A,B and C the following procedure was adopted. An equivalent coaxial cylindrical system was constructed with the inner radius equal to the conductor radius and outer radius equal to the length of the line OJ.

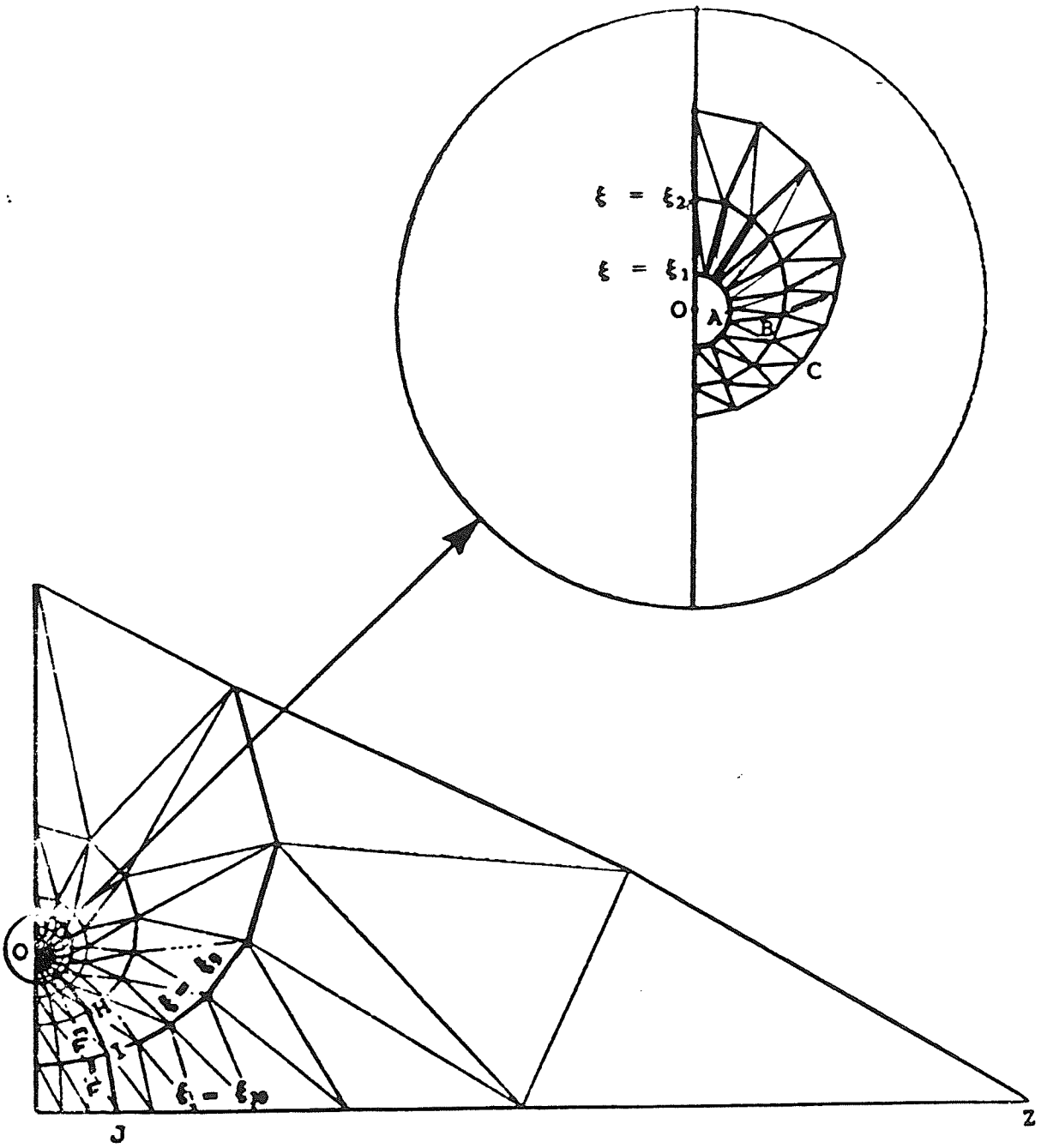

Figure 3.3 Finite Element Mesh

With the potential gradient on the inner conductor chosen to be equal to the approximate corona onset value given by the empirical Peek's formula, the analytical solution for the coaxial cylindrical geometry equation (3.8) was then applied to obtain the initial space charge distribution at any point inside this equivalent coaxial cylindrical system. For example the initial value of ρ at say node C is then easily obtained by finding ρ from equation (3.8) corresponding to a radial distance equal to the length of the line OC. For all nodes lying on the flux line AJ, the value of ρ in equation (3.8) is obtained using equation (3.13) which yields the charge density at the node on the conductor surface lying on the flux line AJ.

The above procedure was followed to determine the initial space charge density at all nodes lying on all lines for which a ground node exists corresponding to a conductor node. Such a situation does not prevail if one considers nodes lying on flux lines which meet the artificial boundary. In these cases the procedure followed was identical except that the outer radius of the equivalent coaxial cylindrical system was chosen to be equal to the length of the line joining the centre of the conductor to the farthest ground node i.e. line OZ.

3.2.3 Steps 3 and 4

In this step equations (3.1)-(3.2) are solved separately by application of the FEM with proper boundary conditions; Φ =V at all conductor nodes, Φ =0 on ground nodes and $\Phi = \Phi_{es}$ at nodes lying on the artificial boundary. The initial value of ρ at all nodes is obtained in step 2. It should be noted that the conductor potential, Φ =V, is that value which corresponds to the experimental values of J at ground level used in step 2 to determine the initial charge distribution in the problem region.

The solution yields the values of E and Φ at all interior nodes.

3.2.4 Step 5 ; application of the proposed algorithm

If the ρ distribution does not correspond to the true value, the solution of field quantities obtained from equations (3.1)-(3.2) will differ. The charge density distribution is therefore updated at all nodes in accordance with an update algorithm which takes into account the location of the nodes. Generally these nodes may be classified into the following categories.

1. Conductor and interior nodes lying on ξ circles(η =constant) at the extremeties of which both conductor and ground nodes are present.

2. Nodes which lie on ξ circles terminating on the artificial boundary including conductor nodes and nodes lying on the artificial boundary.

3. Ground nodes.

Update algorithm for nodes of category 1

The charge density distribution is updated using the scheme

$$\rho^{new} = 0.5\ [\rho^{old} + (\frac{J_m}{J_{1m}+J_{2m}})\ \rho^{co}\ (\frac{\rho^{old}}{\rho^{co}})^{\frac{E_{1c}+E_{2c}}{2E_{2c}}}\ ] \qquad (3.13)$$

where ρ^{new} is the updated value of the volume charge density at any node, ρ^{old} is the charge density at the same node from the previous iteration and ρ^{co} is the value of the charge density at the conductor node lying on the same ξ circle as the node under consideration determined from the previous iteration. E_{1c} and E_{2c} are the electric field intensities determined from equations (3.1)-(3.2) respectively at the conductor node lying on the same ξ circle (η =constant) as the node under consideration. Finally, J_m is the experimental values of J and J_{1m} and J_{2m} are the computed values of J at a ground node which lies on the same ξ circle as the node under consideration.

Update algorithm for nodes of category 2

Under this category, there are three types of nodes. i.e. conductor nodes, interior nodes and nodes lying on the arti-

ficial boundary. For conductor nodes the value of ρ is found by quadratic extrapolation using the most recent values of ρ at the two neighboring conductor nodes.

For other nodes the updating algorithm uses the relation

$$\rho^{new} = 0.5 \left[\rho^{old} + \rho^{c} \left(\frac{\rho^{old}}{\rho^{c}}\right)^{\frac{(E_{1c}+E_{2c})}{2E_{2c}}}\right] \qquad (3.14)$$

where ρ^{c} = most recent value of ρ at the conductor node lying on the same flux line as the node under consideration.

Update algorithm for nodes of category 3

The ρ values at these nodes are updated at the beginning of each iteration(with the exception of the first)using the relation

$$\rho^{new} = 2 \frac{J_m}{k(E_{1m} + E_{2m})} \qquad (3.15)$$

where J_m is the experimental value of J and E_{1m} and E_{2m} are the E field values at ground level obtained from equations (3.1)-(3.2) in the previous iteration.

Equations (3.13) - (3.15) reflect the fact that the space charge distribution is affected not only by the conductor surface potential gradient alone, but also by the combined effect of J and E.

3.2.5 Step 6

Following the first iteration, using the initial ρ distribution, the finite element solution of equations (3.1)-(3.2) is obtained again using the new updated distribution of ρ. This iteration process is continued until the following conditions are simultaneously satisfied at all nodes in the interelectrode region with the exception of nodes lying on the artificial boundary.

$$\begin{aligned} \frac{(\Phi_1 - \Phi_2)}{\Phi_{av}} &\leq \delta_1 \\ \frac{(E_1 - E_2)}{E_{av}} &\leq \delta_2 \\ \frac{(\rho^{new} - \rho^{old})}{\rho^{new}} &\leq \delta_3 \end{aligned} \qquad (3.16)$$

where δ_1, δ_2 and δ_3 are the small deviations specified in terms of the desired accuracy. In this work the values assigned to δ_1, δ_2 and δ_3 were 0.025, 0.03 and 0.025 respectively. In equation (3.16) Φ_1, Φ_2, E_1, E_2 are the potential and field values from equations (3.1) and (3.2). E_{av} and Φ_{av} are obtained by averaging E_1, E_2 and Φ_1, Φ_2 respectively.

3.3 Performance of the proposed algorithm

In contrast to the procedure usually employed to determine the ionized field, the updating scheme does not contain any imposed value for the electric field on the conductor surface and hence the algorithm does not utilize Kaptzov's assumption. However the corona onset gradient at the coronating conductor surface as determined from Peek's formula is necessary to start the iterative process. In all iterations the field intensity on the conductor surface is let free to vary as dictated by the updating algorithm. This yields a field variation on the conductor surface after convergence has been achieved. It was found that about 15 iterations were needed to attain the specified convergence in all field quantities with an accuracy of 2.5% in $|E|$ on the conductor surface and 1% in $|E|$ anywhere in the interior region. The algorithm is therefore efficient and yields good accuracy. For example in reference[2] it is reported that 70 iterations were necessary to obtain an accuracy of 5% in the potential values.

Figure 3.4 shows a detailed flow chart, which includes the steps discussed earlier, which were implemented in order to arrive at field quantities on the surface of a coronating monopolar single conductor given experimental values of ionic current density at ground level.

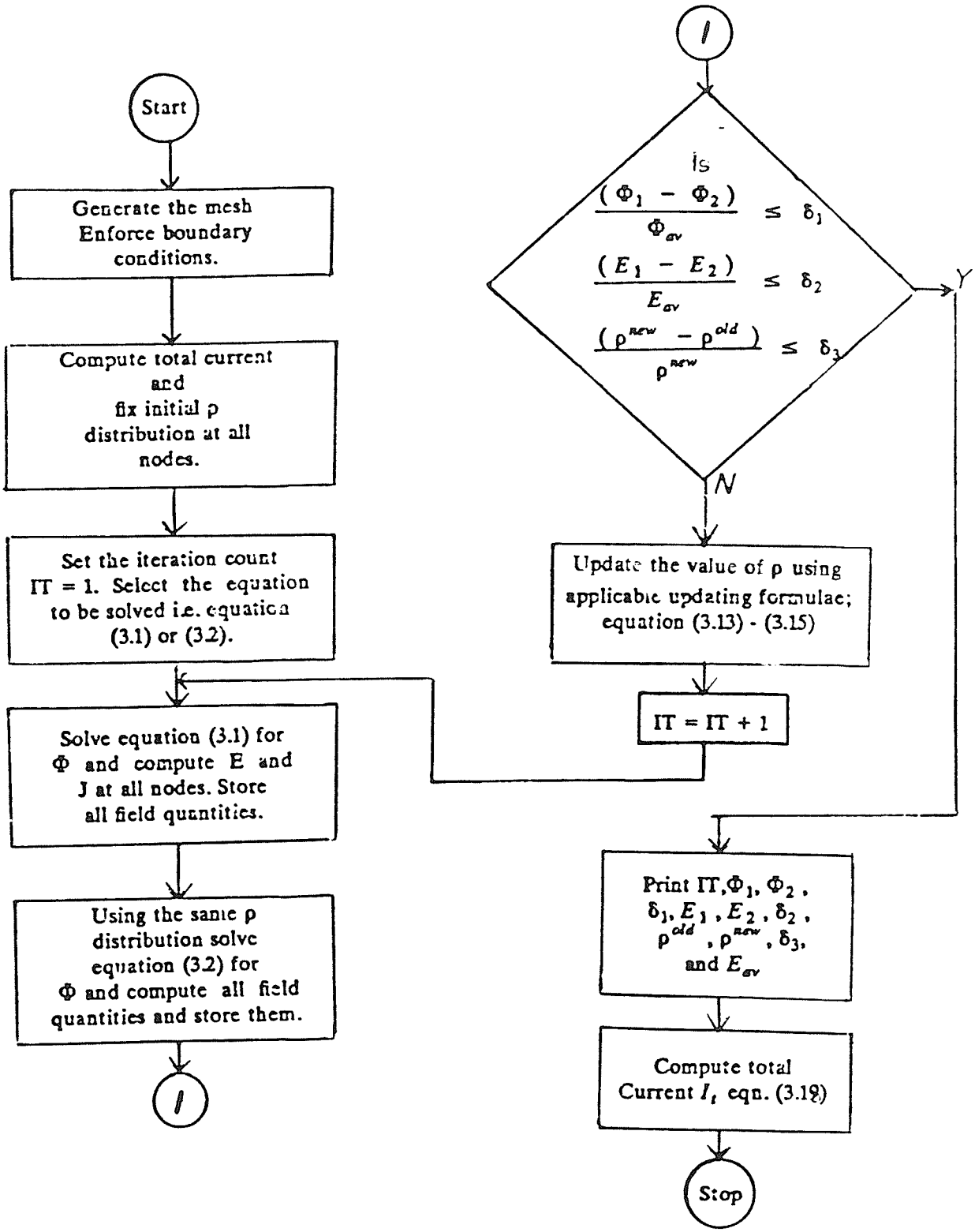

Figure 3.4 Flow chart indicating the steps involved involved in solving the ionized field problem

3.4 Solution, errors and convergence of the iterative process

The method of solution described above was applied to each of the three chosen geometries mentioned earlier in Table 3.1. In all cases the finite element solution was implemented over one half of the total region taking advantage of the problem symmetry; the line of symmetry in all cases being the vertical line joining the centre of the conductor to the ground plane. Along this line the normal derivative of the potential $\frac{\delta \Phi}{\delta n} = 0$.

Initially the errors and convergence rate of the solution was examined in all cases; details are presented below for model 1 only with the conductor energized at +300 kV.

Table 3.3 shows the errors in $|E|$ and Φ along the vertical line joining the conductor centre to ground.

These errors are defined as

$$\text{Error in } \Phi = \frac{(\Phi_1 - \Phi_2)}{\Phi_{av}}$$

$$\text{Error in } E = \frac{(E_1 - E_2)}{E_{av}} \qquad (3.17)$$

The maximum error in potential is 0.591% at height of 177 cm from the ground while the maximum error in $|E|$ is 1.615% which occurs at a height of 60 cm from the ground.

y cm	Φ_1 kV	Φ_2 kV	%Error	E_1 kV/cm	E_2 kV/cm	%Error
0.25	300.00	300.00	0.0	45.38	44.420	2.138
0.40	292.86	292.31	0.188	24.420	24.230	0.781
0.85	285.75	284.86	0.312	13.830	13.650	1.327
1.58	278.65	277.62	0.370	7.189	7.099	1.269
2.90	271.47	269.87	0.591	4.071	3.996	1.26
5.34	263.98	262.89	0.414	2.326	2.321	0.215
9.76	255.27	254.82	0.176	2.156	2.139	0.792
17.00	244.58	244.23	0.143	2.094	2.083	0.526
31.51	227.81	228.66	-0.372	2.014	2.008	0.298
54.61	200.73	200.34	0.194	1.964	1.939	0.770
90.50	155.23	156.649	0.910	1.886	1.864	1.173
140.39	89.808	89.632	0.196	1.873	1.843	1.615
200.0	0.0	0.0	-	1.856	1.838	0.937

Table 3.3 Errors in Φ and E along the line $\theta = 0$

(model 1, Φ=300 kV)

Table 3.4 shows the error in $|E|$ along the ground and around the conductor surface. The position $\theta=0^{\circ}$ corresponds to the point on the conductor surface which lies on the vertical line joining the conductor centre to ground. On the conductor surface the maximum error in $|E|$ occurs at $\theta=0^{\circ}$ and is slightly over 2%; all other errors are less than or equal to 2%. Along the ground, most errors are less than 1%; the maximum error is equal to 2.09% and this occurs at a lateral distance of 8.2m i.e. 4.1 times the conductor height. Figures 3.5 and 3.6 show the variation of the maximum error in potential and maximum deviation in ρ. This latter quantity is the maximum deviation of the ratio $(\rho^{new}-\rho^{old})$ to ρ^{new}. These quantities were calculated at all nodes in the problem region with the exception of nodes on the artificial boundary.

Figures 3.7 and 3.8 show the variation of the computed value of the total corona current I defined by

$$I_t = \frac{\left(\sum_{i=1}^{n} J_i\right) 2\pi r}{n} \qquad (3.18)$$

and the variation of the average value of the electric field on the conductor surface, E_{avg}, versus the number of iterations. At each node on the conductor surface the electric field is obtained by averaging E_1 and E_2. The average of this quantity over all conductor nodes is E_{avg}.

θ	E_1 kV/cm	E_2 kV/cm	%Error	x m	E_1 kV/cm	E_2 kV/cm	%Error
0.00	45.38	44.42	2.138	0.0	185.7	183.9	0.987
12.85	45.39	44.51	1.958	0.225	184.0	182.5	0.805
25.66	45.42	44.58	1.867	0.456	182.1	179.8	1.28
38.51	45.46	44.64	1.82	0.700	168.8	167.6	0.663
51.37	45.49	44.69	1.772	0.859	164.3	164.1	0.150
64.2	45.53	44.75	1.728	1.259	149.2	148.2	0.678
77.06	45.61	44.81	1.769	1.595	135.2	134.5	0.539
90.0	45.63	44.87	1.679	2.0	119.0	117.4	1.430
102.74	45.70	44.90	1.766	2.51	107.6	105.9	1.59
115.62	45.68	44.86	1.813	3.20	81.76	81.08	0.836
128.47	45.62	44.82	1.77	4.15	63.21	62.54	1.069
141.38	45.58	44.76	1.817	8.20	29.54	28.92	2.09
154.23	45.57	44.73	1.862				
167.12	45.52	44.70	1.820				
180.0	45.51	44.61	2.00				

Table 3.4 Error in $|E|$ around the conductor surface and along ground (model 1, Φ = 300 kV)

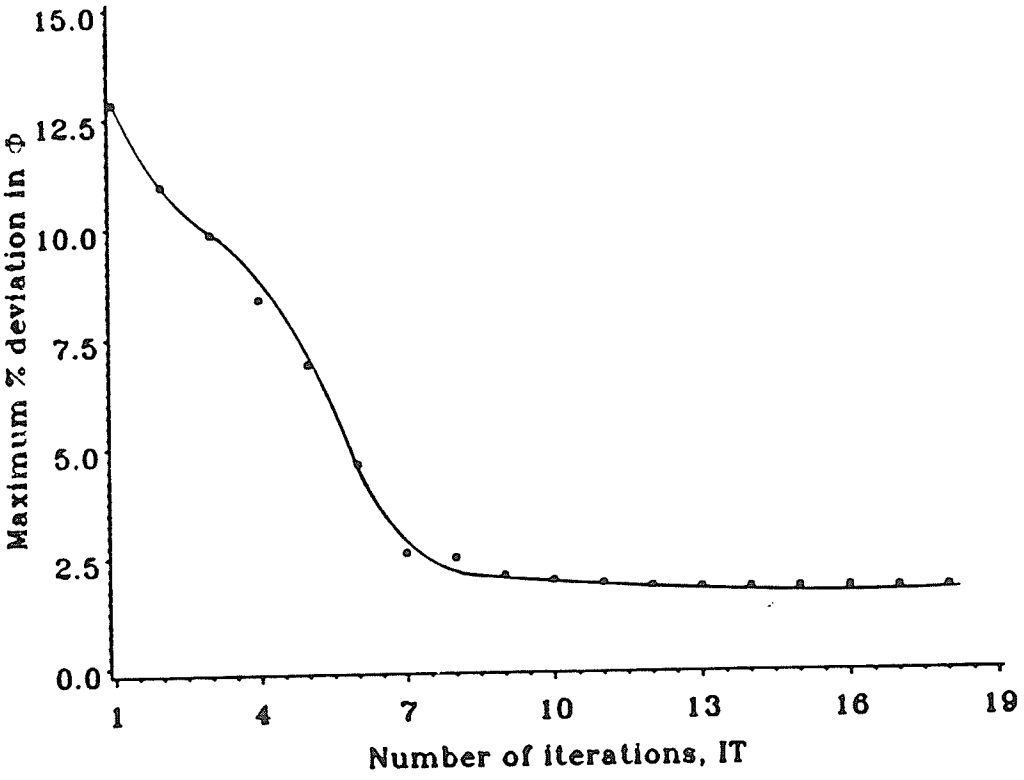

Figure 3.5 Maximum deviation in nodal potential vs number of iterations (model 1, Φ = 300 kV)

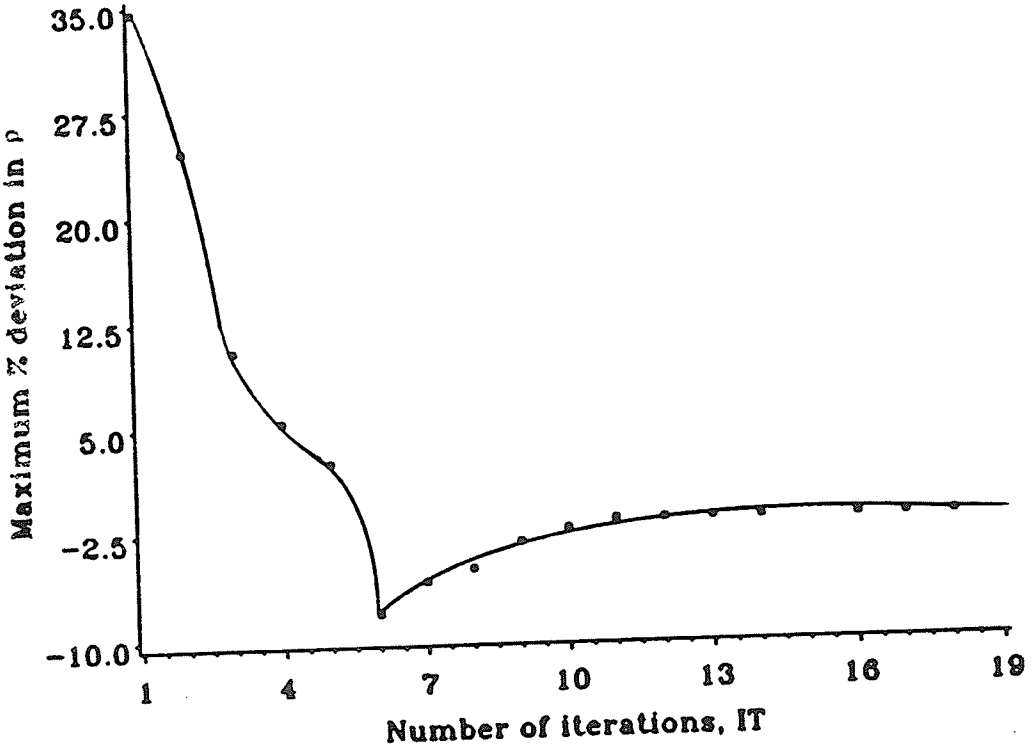

Figure 3.6 Maximum deviation in ρ values vs number of iterations (model 1, Φ = 300 kV)

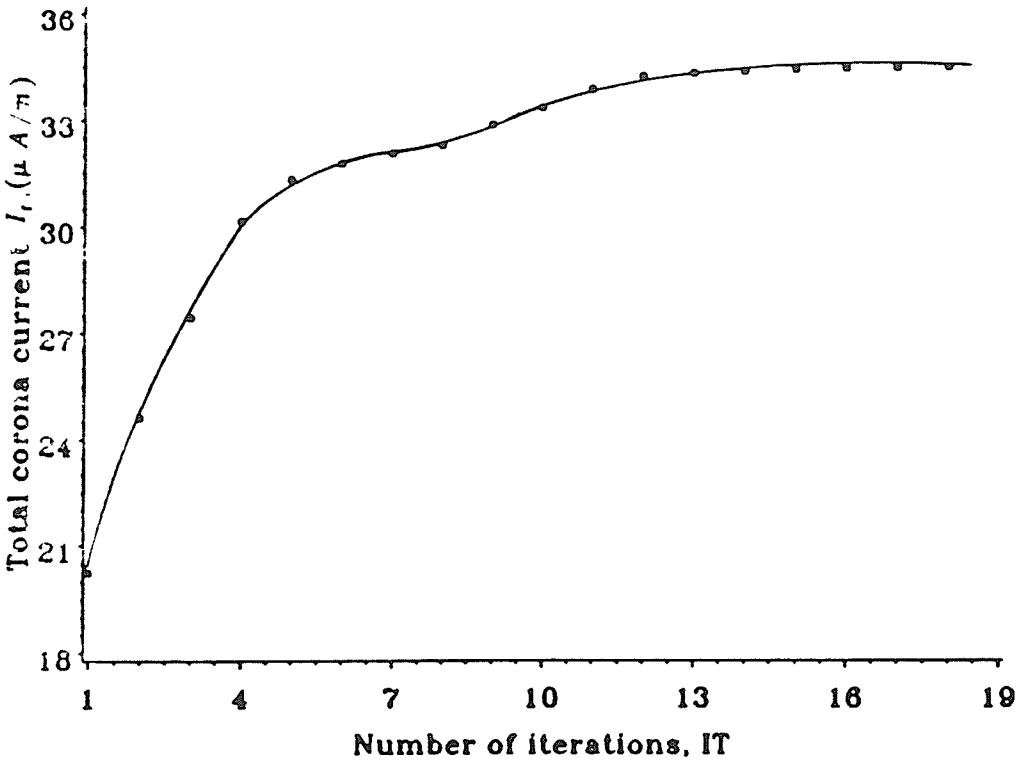

Figure 3.7 Variation of total current vs number of iterations (model 1, Φ= 300 kV)

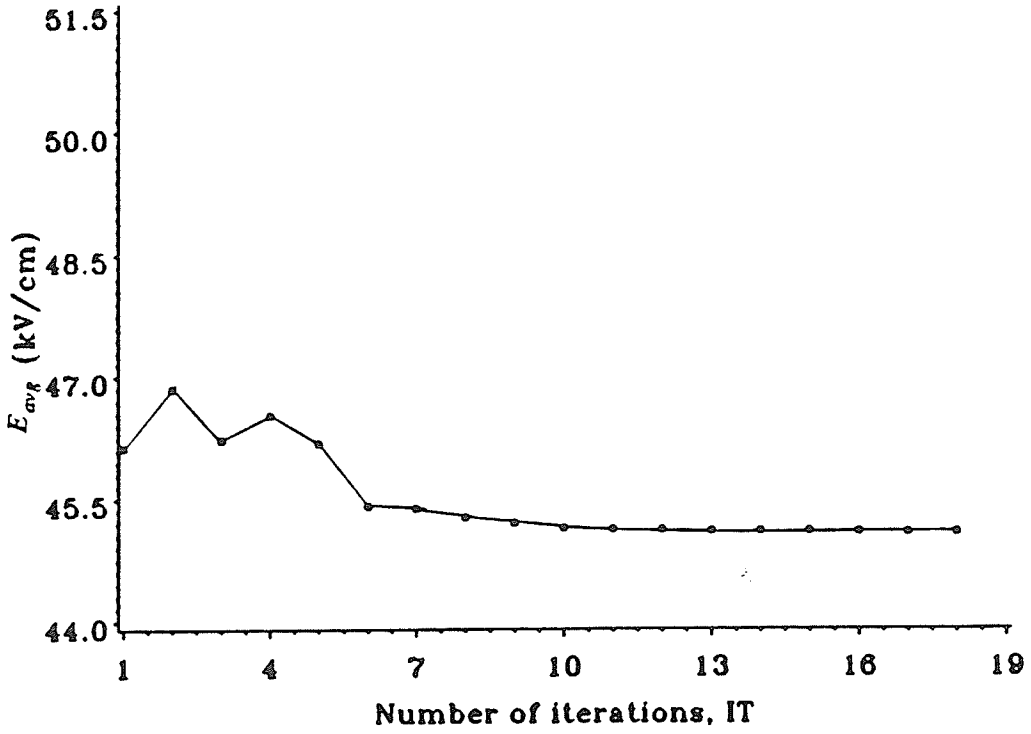

Figure 3.8 Variation of average conductor surface gradien
vs number of iterations
(model 1, Φ = 300 kV)

3.5 Variation of field quantities on and around conductor surface for model 1 (positive polarity)

Figures 3.9,3.10 and 3.11 show the variation of ρ ,J and $|E|$ around the conductor surface when the conductor is energized at a polarity with a voltage of 300 kV. The electric field values at the conductor nodes are the average values of E_1 and E_2. The ionic current density values were obtained by computing the value of $k \rho E_{av}$ at each node.

From Figure 3.9, ρ is maximum at $\theta = 0^{\circ}$ and minimum at $\theta = 180^{\circ}$, as expected. From Figure 3.10 J is maximum at $\theta = 0^{\circ}$ and minimum at $\theta = 180^{\circ}$. The variation of J with θ is quite similar to that of ρ thus indicating that E_{av} does not a exhibit large variation with angular position.

From Figure 3.11 it is seen that E_{av} peaks at $\theta = 102^{\circ}$; the minimum occurs at $\theta = 0^{\circ}$. The value of E_{av} at $\theta = 0^{\circ}$ is less than that at $\theta = 180^{\circ}$. The average value of the conductor gradient E_{avg} is 45.12 kV/cm which is 11.26% below the onset gradient, E_o, as determined from Peek's formula. The difference between the values of E_{av} at $\theta = 0^{\circ}$ and $\theta = 180^{\circ}$ and the average value of the conductor gradient , E_{avg}, expressed as a percent of E_{avg} is 0.488 and 0.124% respectively. The value of $(E_{max.} - E_{min.})/E_{avg}$ is 0.755% which is greater than the corresponding value for the electrostatic field, i.e. 0.133%.

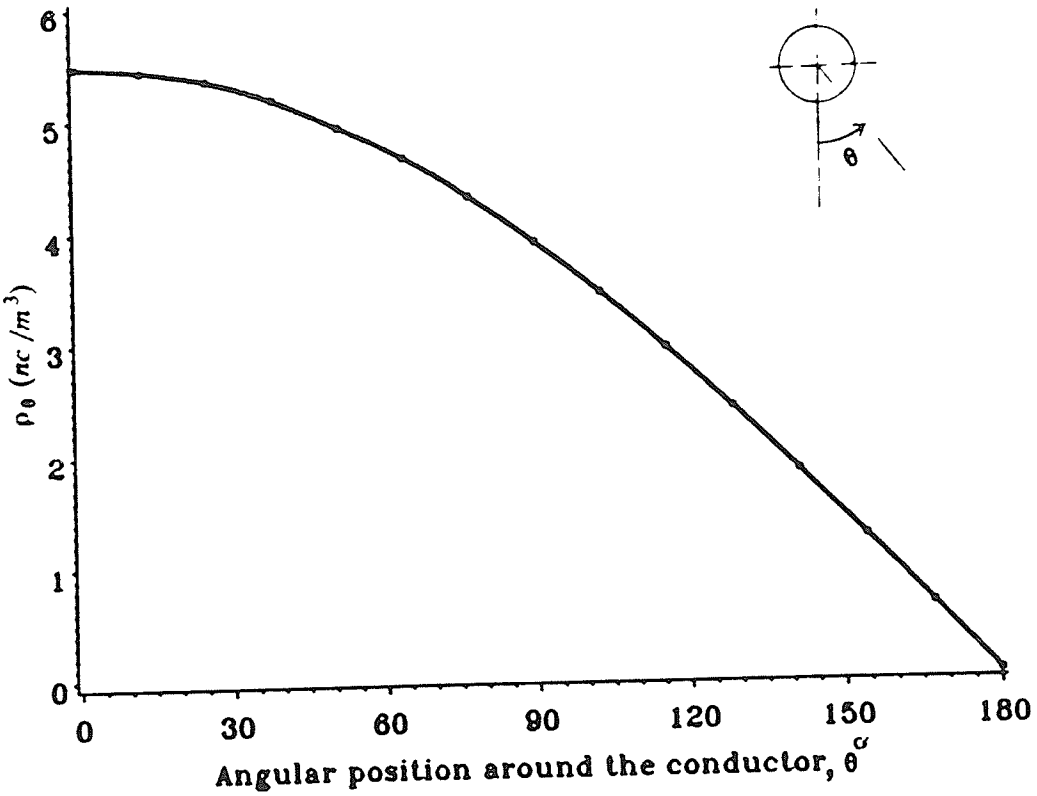

Figure 3.9 Variation of ρ around the conductor (model 1, Φ =300kV)

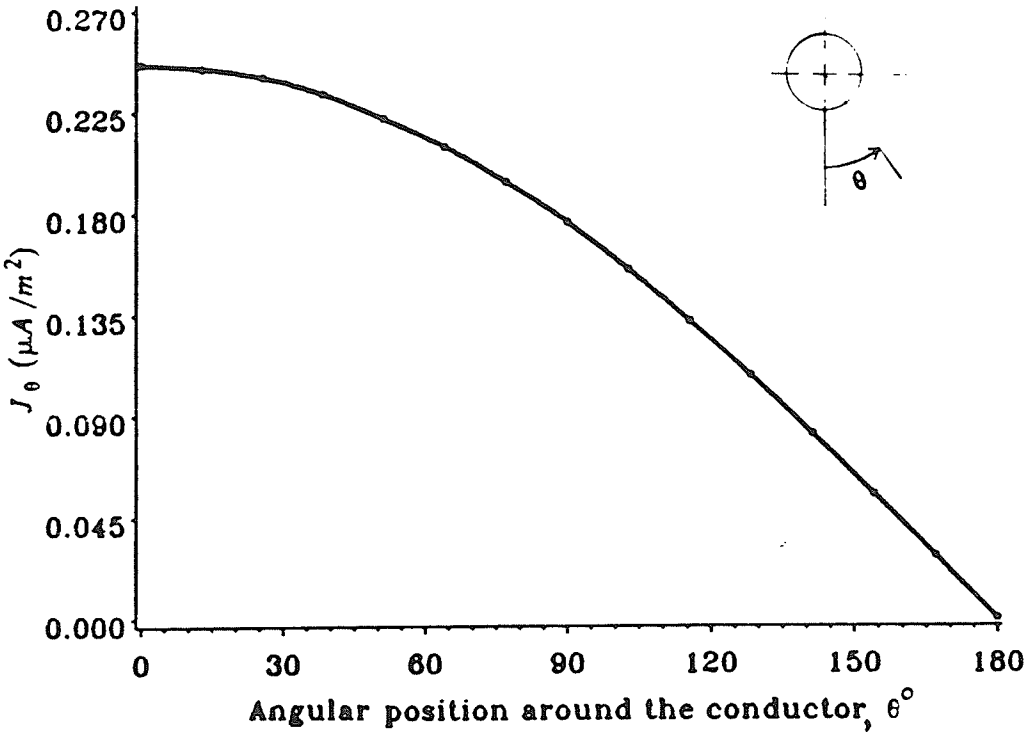

Figure 3.10 Variation of J around the conductor (model 1, Φ = 300 kV)

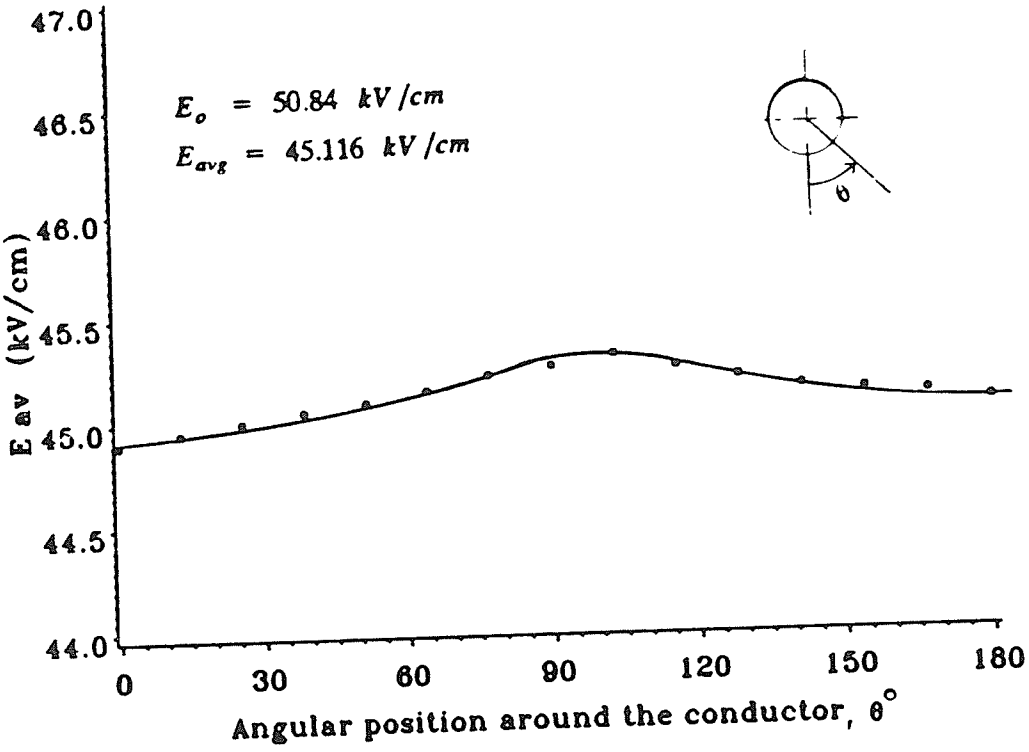

Figure 3.11 Variation of conductor surface gradient (model 1, Φ= 300 kV)

From reference [8] data concerning J at ground level was also available at Φ = 200 kV. and it was therefore possible to calculate the variation of E_{av} around the conductor surface at this voltage. Although data was also available in reference[8] for Φ =100 kV, a similar calculation could not be performed due to the difficulty in obtaining current density values at ground level from the graph provided. Figure 3.12 shows the variation of E_{av} vs θ for Φ =200 kV. From this Figure it is seen that E_{av} peaks once again at $\theta = 102^{\circ}$ the minimum value of E_{av} occurs at $\theta = 0^{\circ}$. The average value of the conductor gradient E_{avg} is 46.05 kV/cm which is 9.42% below E_o as determined by Peek's formula.

Since the variation of the electric field around the conductor surface is of the same order as the errors in $|E|$ reported in Table 3.4 on page 59, one may be tempted to conclude that the reported variation with angular position of the conductor gradient on the coronating conductor's surface is of doubtful validity. However, this is not the case. An examination of the results showed that the errors in the computed value of the electric field are in the same direction at all nodes i.e. all positive. It is therefore possible to conclude that Figure 3.11 represents the nature of the variation of the electric field variation of the electric field with angular position to an accuracy of 2%.

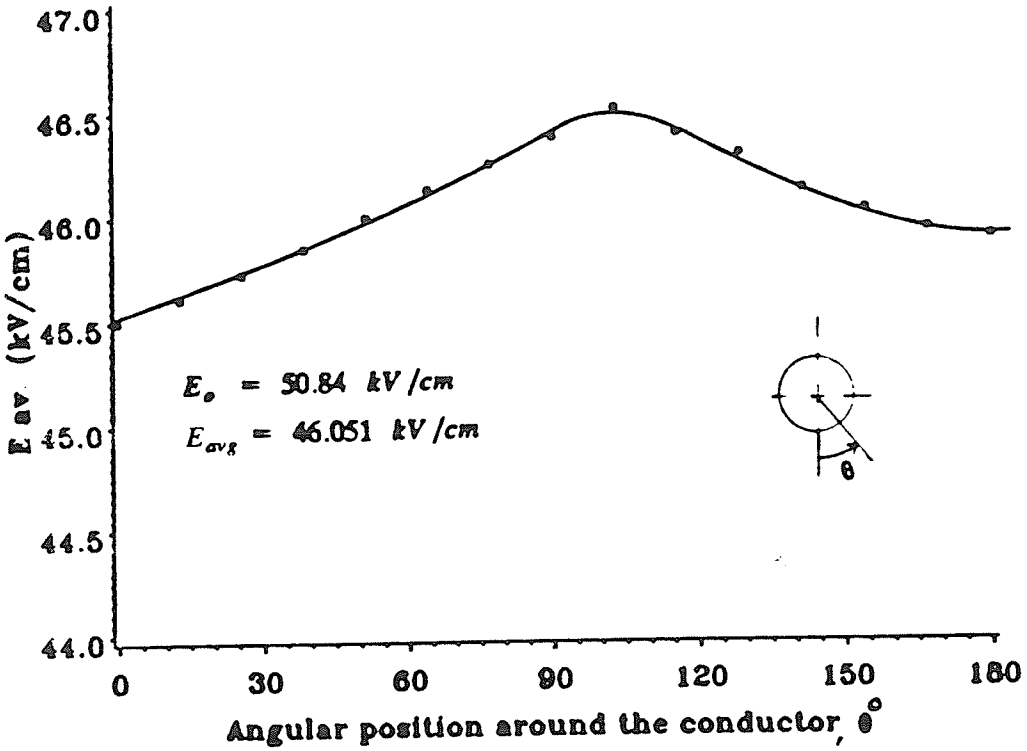

Figure 3.12 Variation of conductor surface gradient (model 1, Φ=200 kV)

3.6 Effect of the voltage level on the field variation around the conductor surface

From Figures 3.11 and 3.12 it is seen that although the conductor voltage has decreased by 33%, the average value of the conductor gradient E_{avg} increases only by 1.84%. Also it is seen that the variation of E_{av} with θ around the conductor periphery is more pronounced at Φ=200 kV. Figure 3.13 indicates the variation of the quantity $\frac{(E_{avg} - E_o)}{E_o}$ as a function of the applied voltage. At $\Phi = \Phi_o$=93.8 kV the electric field is equal to the onset value calculated from Peek's formula. As the voltage is increased beyond the onset value the deviation of the E_{avg} from the onset gradient E_o increases nonlinearly. The slope of the curve of Figure 3.13 decreases and eventually approaches zero. In figure 3.13 a smooth curve has been drawn through 3 points corresponding to Φ_o,200 and 300 kV. It is seen that the slope of the curve decreases and eventually approaches zero.

3.7 Discussion of results

The above results show that the electric field on the coronating conductor surface does vary with position, and that the percentage variation depends on the applied voltage. The greater the voltage the lesser the variation. Also the average value of $|E|$ on the conductor surface is lesser than that calculated by Peek's formula. As the voltage is increased beyond onset the average conductor gradient, E_{avg} drops noticeably at first but this trend does not

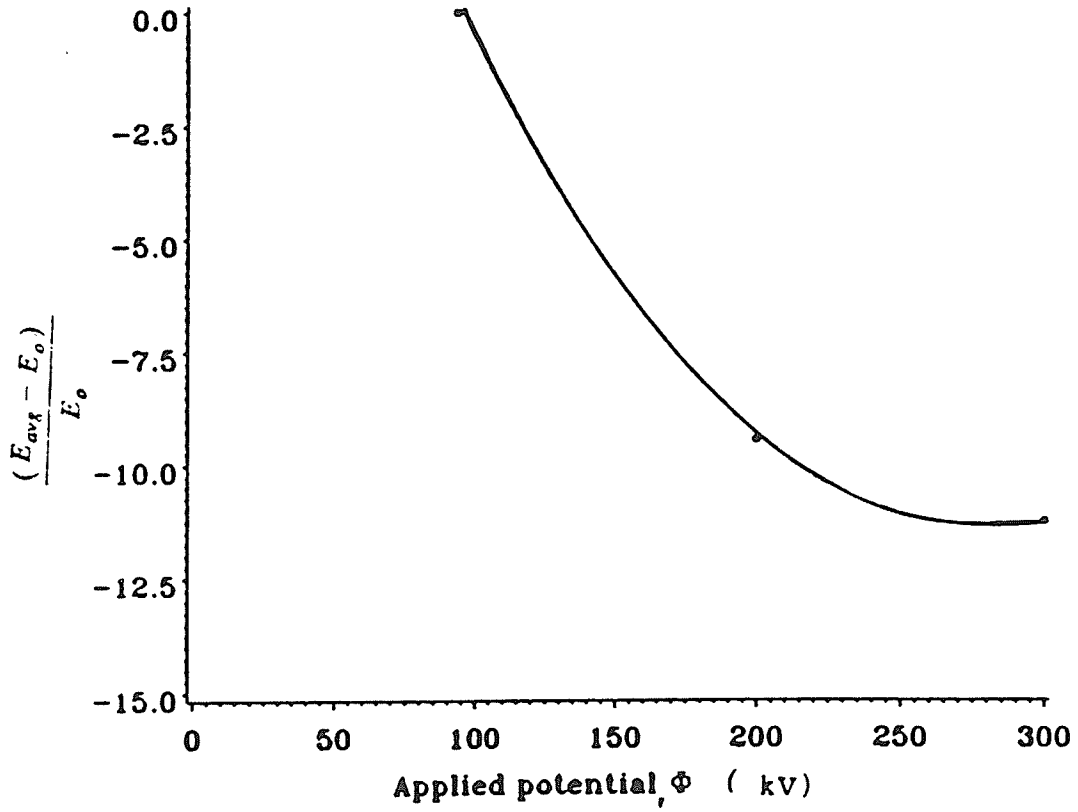

Figure 3.13 Deviation of average conductor surface gradient from E_o as a function of the applied voltage

continue indefinitely; eventually, E_{avg} stabilizes at a particular value.

These findings reported in Figures 3.11 and 3.13 are supported by consideration of the physical process of corona.

With a positive coronating conductor, space charge of like polarity surrounds the conductor. In the steady state this layer is responsible for the lowering of potential gradient from the onset value. This effect is more pronounced where the space charge density is greatest i.e. $\theta = 0^{\circ}$. Hence the conductor gradient registers a minimum at this point(Figure 3.11). In order to explain, qualitatively, the shape of the curve in Figure 3.13 one has to consider the angular variation of ρ and the electrostatic conductor gradient. At $\theta = 180^{\circ}$ the space charge density is weak and the electric field is not affected much. In between, at $\theta = 102^{\circ}$ the charge density is greater than at 180° but so is the electrostatic gradient. These two factors combine in such a manner so as to yield a maximum.

The trend exhibited by Figure 3.9 can also be explained qualitatively. As the applied voltage is increased beyond the onset value the density of the space charge in the ionization layer increases dramatically resulting in a noticeable drop in the average value of the conductor gradient from its onset value; with a further increase in the applied voltage the space charge density increases but not in

the same proportion. Eventually the ionization layer may be considered to be saturated with space charge. At this point the average conductor gradient stabilizes.

3.8 Models 2 and 3(positive polarity)

Data available in references [2] and [15] were used to calculate the variation of E around the conductor surface in both cases as shown in Figures 3.14 and 3.15. These Figures show that the variation is similar to that shown earlier. The value of E_{avg} are once again lower than the onset values calculated by Peek's formula. Table 3.5 summarizes some salient features which emerge from the analysis of the three models.

3.9 Results with -ve polarity

Experimental data was available in reference[8] concerning model 1 for -ve polarity at conductor voltages of 200 and 300 kV. A procedure similar to that adopted for the positively charged conductor was followed. The only change is that the mobility k^-, of negative ions, has to be used instead of k^+. In this study k^- was chosen to be 1.8 cm^2/Vs [8]. It was found that the average value of the conductor surface gradient, E_{avg}, was lower than the onset gradient as calculated from the Peek's formula; In fact the results

	Model 1	Model 2	Model 3
Reference	[8]	[2]	[15]
H	200 cm	40 cm	25 cm
r	0.25 cm	0.165 cm	0.056 cm
H/r	800	242	446
Φ	200,300	80	50
Onset voltage	93.8kV	56.55 kV	27.75 kV
Φ/Φ_o	2.13,3.2	1.42	1.802
+ Onset grad.	50.84	55.42	72.92
- Onset grad.	52.92		
E_{avg}	46.051,45.116	48.4	62.87
$\frac{(E_{avg} - E_o)}{E_o}$	9.42,11.26%	12.26%	13.78%

Table 3.5 Some salient features resulting from the analysis of three models

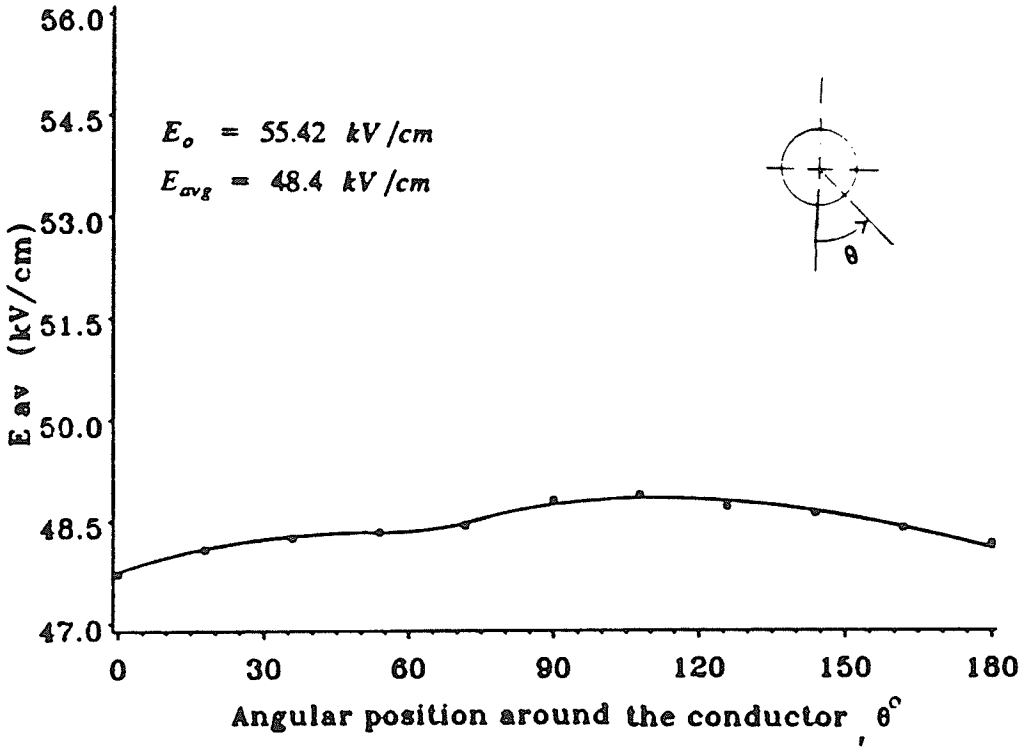

Figure 3.14 Variation of conductor surface gradient (model 2, Φ=80 kV)

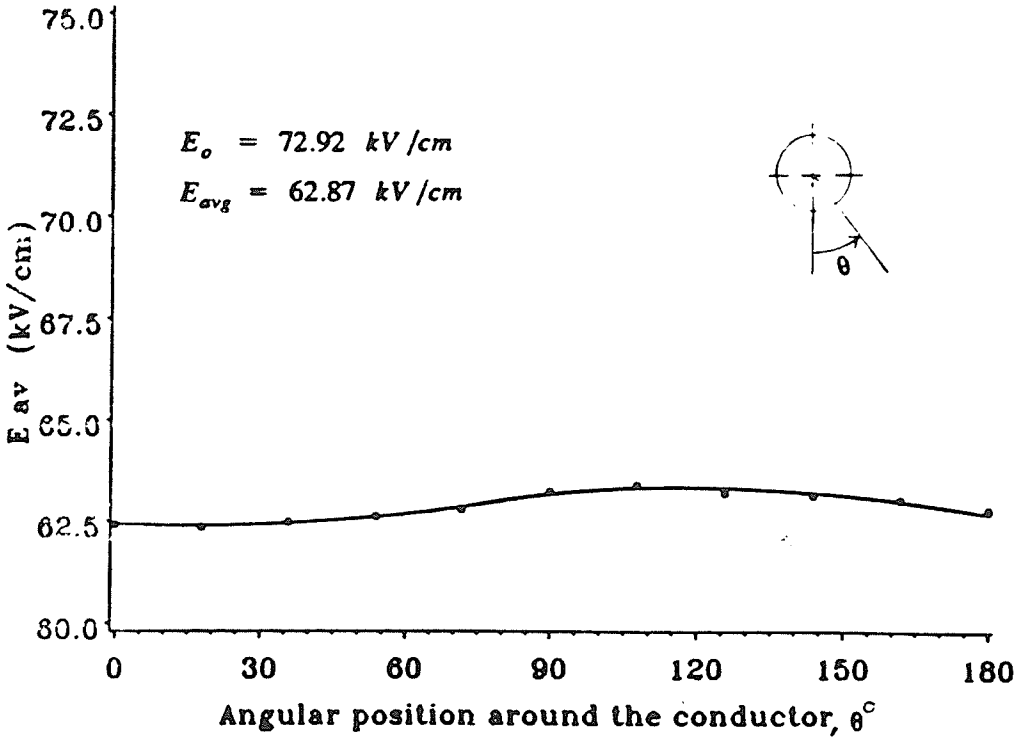

Figure 3.15 Variation of conductor surface gradient (model 3, Φ=50 kV)

obtained were similar in character to those obtained with the conductor energized at positive polarity.

These results can not be justified from physical considerations. With a negatively charged coronating conductor it is known that, in the steady state, the presence of the positive space charge in the ionization layer contributes to an increase in the value of the conductor surface gradient.

In the analysis, however, the positive space charge is not considered at all which accounts for the fact that an increase in the average value of the E field is not shown by calculations.

However, since the positive space charge may be considered to occupy a thin layer surrounding the coronating electrode, the thickness of which is usually three orders of magnitude smaller than the interelectrode distance,[21], the computed values of the electric field on the conductor surface may be considered to be applicable at the edge of the ionization layer.

Chapter IV

CONCLUSIONS

The results of this study show that following onset of corona, the electric field at the surface of a monopolar single conductor does not remain constant at the onset value. With a positively charged conductor, the average surface electric field decreases from the onset gradient. As the conductor voltage is increased above the onset voltage, this decrease is rapid at first but eventually the average conductor gradient stabilizes at a particular level. The electric field also varies around the periphery of the conductor surface; the extent of variation, which increases with the applied voltage, is small when compared to the drop in the value of the average conductor surface gradient from the onset gradient as provided by Peek's formula. The experimental results of Popkov[15] support the conclusions arrived at for positive polarity. Popkov's experimental work utilized the geometry of model 3.

The computations performed with a negatively charged conductor indicate results similar to those obtained with positive polarity. It has been pointed out that this is not correct and is, infact, in contradiction with results expected from consideration of the physical process. This oc-

curs because, the steady state model ignores the presence of positive space charge which is responsible for the increased conductor gradient.

Finally, the conclusions drawn from positively charged conductor enable one to appreciate the reason for the occurrence of rather large errors in electric field values on the conductor surface in conventional ionized field analysis of monopolar single conductor geometries. In such an analysis, one usually invokes the Kaptzov assumption and solves for field quantities at ground level. Since the Kaptzov assumption is unrealistic one should, logically, not expect small errors in the electric field on the coronating conductor's surface.

REFERENCES

1. Abdel-Salam, M. and Khalifa, M., "Considering Space Charge in Calculations of Monopolar DC Corona Loss", Acta Physica Academiae Scientiarum Hungaricae Tomus 36(3), pp. 201-214, 1974.

2. Abdel-Salam, M., Farghally, M. and Abdel-Sattar, S., "Finite Element Solution of Monopolar Corona Equation", IEEE Trans. EI, vol. EI-18, No. 2, April 1983.

3. Bathe, K. FINITE ELEMENT PROCEDURES IN ENGINEERING ANALYSIS, PRENTICE-HALL, INC., Englewood Cliffs, NJ

4. Ciric, I. R. and Kuffel, E., "On the Boundary Conditions for Unipolar DC Corona Field Calculation", Int. Symposium on High Voltage Engineering Athens-Greece, 5-9 Sept. 1983.

5. Felici, N.J., "Recent Advances in the Analysis of DC Ionized Electric Fields", Direct Current Part I; Sept. 1963 pp. 252-260, Part II; Oct. 1963 pp. 278-287.

6. FlatabØ, N., "Transient heat conduction problems in power cables solved by the finite element method", IEEE PAS, pp. 56-63, 1973.

7. Gela, G., "Computation of Ionized Fields Associated with Unipolar DC Transmission Systems", Ph. D. thesis, Department of Electrical Engineering, University of Toronto, April 1980.

8. Hara, M., Hayashi, N., Shiotuski, K., and Akazaki, M., "Influence of Wind and Conductor Potential on Distributions of Electric Field and Ion Current Density at Ground level in DC High Voltage Line to Plane Geometry", IEEE Trans. PA & S, vol. PAS-101, No. 4, April 1982.

9. Janischewskyj, W. and Gela., G "Finite Element Solution for Electric Field of Coronating DC Transmission Lines", IEEE Trans. , vol. PAS-98, pp. 1000-1012, May/June 1979.

10. Janischewskyj, W., Sarma Maruvada, P. and Gela, G., "Corona Losses and Ionized Fields of HVDC Transmission Lines", CIGRE-session, Paris, France, 1-9 Sept. 1982, Paper 36-09.

11. Maruvada Sarma, P. and Janischewskyj, W., "Analysis of Corona Losses on DC Transmission lines , Part I, Unipolar Lines", IEEE Trans. PA & S, vol. PAS-88, No. 5, May 1969, pp. 718-731.

12. McDonald, B.H. and Wexler, A., "Finite Element Analysis of Unbounded Field Problems", IEEE Trans. MTT, vol. MTT-20, pp. 841-847, Dec. 1972.

13. Parekh, H., Chow, Y.L. and Srivastava, K.D., "A Simple method of Calculating Corona Loss on Unipolar DC Transmission Lines", IEEE Trans. EI, vol. EI -15 No. 6, December 1982

14. Peek, F.W., "Dielectric Phenomena in High Voltage Engineering, McGraw-hill 1929.

15. Popkov, V.I., "On the Theory of Unipolar DC Corona", Elektrichestvo, NRC TT-1093 , No. 1, pp. 33-49, 1949.

16. Silvester, P. and Hsieh, M.S., "Finite-Element Solution of 2-dimensional Exterior Field Problems", Proc. IEE 118, pp. 1743-1747, 1971.

17. Tadasu Takuma, Tsutomu Ikeda and Tadashi Kawamoto, "Calculation of Ion Flow Fields of HVDC Transmission Lines by the Finite Element Method", IEEE Trans. PA & S, PAS-100, No. 12, December 1981.

18. Venkatesha, M.K., Raghuveer, M.R. and Ciric, I.R, "Accuracy of the Finite Element Electrostatic Field Solution of a Monopolar DC Transmission Line Model", Int. conference on Computers, Systems and Signal Processing, Dec. 9-12, 1984, Bangalore, India pp 674-678.

19. Wexler, A., Finite Elements for Technologists Dept. of Elect. Eng., University of Manitoba, TR 80-4 1980.

20. Electrostatic and Electromagnetic effects of UHV Transmission Lines EPRI EL-802 Project 566 Final Report June 1978.

21. Transmission line Reference book HVDC to ±600 kV, pp. 19.

Appendix A

FINITE ELEMENT ANALYSIS

In this appendix, the basic principles of the Finite Element Method are discussed. Over the years, this method has developed into a very appealing, powerful and flexible approach to obtain numerical solutions of boundary value problems. It must be stressed that only two boundary conditions are required to solve a boundary value problem described by a second order differential equation. The third boundary condition is an essential part of the formulation of the ionized field problem. In this work it is employed to compute the initial and subsequent values of space charge density after every iteration.

The standard way of numerically solving the boundary value problem consists of superimposing a suitable grid over the region of interest and locally fitting the known basis functions. By doing so the differential equations are transformed into set of algebraic equations which can be solved for the unknown variables.

For the sake of convenience the equations governing the monopolar corona can be written as

$$\nabla \cdot (\alpha \nabla \Phi) = \beta \qquad (A.1)$$

The quantities α, Φ and β are functions of space coordinates which represent the region Ω. The solution is accomplished through the use of variational FEM. The preliminary step in the VFEM is the formulation of the functional. However, the requirement of the variational equivalent of the differential equation limits significantly the types of the problems to which the concept of finite elements may be applied.

Application of FEM proceeds by first discretizing the region of interest Ω into smaller subregions. Most often, the subregions are triangular in shape. In 3-d problems tetrahedrons are used. The attention is confined only to 2-dimensional regions of interest and is focussed on the methods for the minimization of the functional of the form

$$F = \int_{\Omega} (\alpha (\nabla \Phi)^2 - 2 \beta \Phi) \, d\Omega \qquad (A.2)$$

Trial functions are constructed in a piecewise manner. As in any variational method, approximate finite element solutions are obtained through extremization of the functional. This requires the first derivative of the functional with respect to all the variational parameters be zero, which is a necessary condition for stationarity. An algebraic system of equations is formed whose solution give an approximate solution to the problem under consideration.

A.1 Isoparametric transformation

Consider the use of the 2nd order quadratic finite elements. Same set of functions is used to map the master element from the local simplex to the global coordinates and also for the expansion of the unknown potential within the element. In order to transform the triangular simplex, following transformations are introduced.

$$\begin{cases} x = \sum_{i=1}^{6} x_i \alpha_i \ (\xi,\eta) \\ y = \sum_{i=1}^{6} y_i \alpha_i \ (\xi,\eta) \end{cases} \tag{A.3}$$

In the ξ - η simplex, the unknown function Φ with in the element is approximated by using the same shape functions as

$$\Phi \ (\xi,\eta) = \sum_{i=1}^{6} \Phi_i \ \alpha_i \ (\xi,\eta) \tag{A.4}$$

where $\alpha \ (\xi \ ,\eta)$ are the Lagrangian shape functions defined under the node numbering scheme in Figure 4.1 are given by

$$\begin{cases} \alpha_1(\xi,\eta) = 2(1-\xi-\eta)\,(1/2-\xi-\eta) \\ \alpha_2(\xi,\eta) = 2\,\xi\,(\xi-1/2) \\ \alpha_3(\xi,\eta) = 2\,\eta\,(\eta-1/2) \\ \alpha_4(\xi,\eta) = 4\,\xi\,\eta \\ \alpha_5(\xi,\eta) = 4\,\xi\,(1-\xi-\eta) \\ \alpha_6(\xi,\eta) = 4\,\eta\,(1-\xi-\eta) \end{cases} \tag{A.5}$$

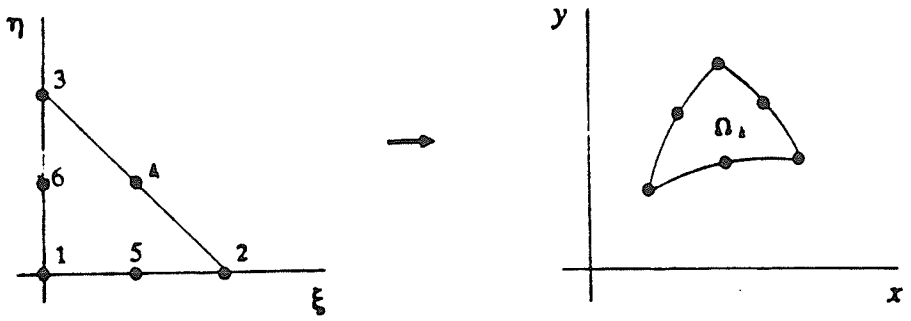

Figure A.1 Mapping of the quadratic element.

All the necessary calculations are can be done in the local simplex using transformations (A.3). The compatibility can be ensured by assigning the same coordinates and the potential value to the nodes that are shared by adjacent elements. Assuming the transformation does not entail excessive distortion of the element, the mapping is one to one.

A.2 Seeking a stationary point

In fact, numerically it is rarely possible to ensure the total arbitrariness of Φ and so, the stationary point located will approximate the solution. Since a stationary point corresponds to a solution, and since there can not be more than a single solution for a positive definite operator, it is clear that there is only a single stationary point of the functional.

In the ξ-η simplex, the unknown function Φ within the element k is approximated using same set of shape functions as

$$\Phi(\xi,\eta) = \sum_{i=1}^{6} \Phi_i^k \alpha_i(\xi,\eta)$$

with the domain Ω divided into N subregions the functional becomes

$$F = \sum_{k=1}^{N} \int_{\Omega_k} [\kappa \sum_{i=1}^{6} \sum_{j=1}^{6} (\nabla \alpha_i^k . \nabla \alpha_j^k) - 2\beta \sum_{i=1}^{6} \Phi_i^k \alpha_i^k] d\Omega \quad (A.6)$$

For the extremization of the functional, one requires the derivatives of (A.6) with respect to all of the variational parameters be zero. The variational parameters are the nodal potentials Φ_i^k that are unknown.

$$\delta F / \delta \Phi_i^k = \int_{\Omega_k} [\kappa \sum_{j=1}^{6} (\nabla \alpha_i . \nabla \alpha_j) \Phi_j - \beta \alpha_i^k] \qquad (A.7)$$

Using (A.6) and (A.7) and identifying those Φ_i^k that are unknown, one then obtains a system of simultaneous equations from which the unknowns Φ_i^k can be solved.

All integrations will be performed in the local ξ-η simplex. This makes the finite element analysis systematic and allows the application of standard quadrature formulae that are readily available.

To test the feasibility of the proposed algotithm number of cases were tested. The program written in FORTRAN was developed and all cases were tested on Amdahl 5850 system at the University of Manitoba. The program listed in Appendix B can be used to solve any equation of the kind $\nabla .(\alpha \nabla \Phi) = \beta$. α and β can be chosen according to the type of equation being solved. The total number can changed by varying IT. The amount of CPU time required to solve is problem depen-

dent. Discretization and the type of the element also play a vital role. The program stores the elements on and below the main diagonal. The data input sheet is furnished which makes the program user's friendly. The program listed in Appendix C would draw the mesh for a given set of node coordinates and numbering. Appendix D gives the storage scheme employed by the Finite Element Program listed in Appendix B.

Appendix B

FINITE ELEMENT PROGRAM

```
//VENKA  JOB ',L=30,,,T=32M',CLASS=1
//  EXEC WATFIV,SIZE=3900K
//SYSIN DD *
     JOB WATFIV  VENKA,NOEXT,NOWARN
C
C
C.....REF: IEEE TRANSACTIONS OF PA AND S
C
C
C.....AUTHOR: MASANORI HARA (JAPANESE)
C
C
C.....DATA AVAILABLE: J-GROUND  AND I-TOTAL
C
C
C.....CONFIGURATION: CONDUCTOR TO PLANE.
C
C
C.....R=0.25 CM, H=200.0 CM, V=-300KV, H/R=800.00, IT=39.85 MUA//M/
C
C
C.....MU=199.99937,UO=7.37
C
C
C.....MESH HAS 121 PRINCIPLE NODES WITH 199 ELEMENTS. THERE ARE
C
C
C.....11 CONDUCTOR NODES. TDN=40, TN=440, CPU TIME=3 MINUTES 40 SEC
C
C
      REAL  GPX(9),GPY(9),W(9),J(9,2,6),AGP(9,6),XX(727),YY(727)
     *    ,XG(6),YG(6),S(727,727),DV(75),C(727),EA,J11(9),J12(9),
     *     J21(9),J22(9),EPSI(10),DET(9),AA(9),BB(9),CC(9),DD(9)
     * ,EE(9),FF(9),F,ES,RO(10),ROU(727),C1(727),C2(727),C3(727)
     *,ROV(727),C23(727),U1(727),U2(727),U3(727),U4(727)
     *,RM2(727),RM3(727),THETA2(727),THETA3(727),ETA(727)
      REAL U5(727),R(6),O(5,5),WARA(15),PX(150),AITA(727),
           YMN(800),PP(800),YND(800),EP(382),DP(800),EPN(800),
     # EFL(182),EMTP(800),RNA(500)
      INTEGER E(335,6),TE,TN,TDN,DN(75),T,Z,U,TALT,TAD,H,LIST(800)
      COMMON/VENKA/A(230000),B(750),MAXA(700),N,NN,NWA,KKK
      PI=3.14159
      ALPHA=  1.0
```

```
      BEETA=1.0
      READ,TE,TN,TDN,TALT,TAD,NGP
C     PRINT 301,TE,TN,TDN,TALT,TAD,NGP
 301  FORMAT('0',10X,6I8)
      READ,((E(M,N),N=1,3),M=1,TE)
C     PRINT 302,((E(M,N),N=1,3),M=1,TE)
 302  FORMAT('0',10X,3I8)
      READ,(XX(I),YY(I),I=1,TN)
C     PRINT 303,(XX(I),YY(I),I=1,TN)
 303  FORMAT('0',10X,2F15.8)
C     GENERATE SECONDARY NODES
      NN=1
      DO 51 I=1,TE
         NC=3
         DO 52 M=1,2
            MM=M+1
            DO 53 N=MM,3
               NC=NC+1
               XS=(XX(E(I,M))+XX(E(I,N)))/2.0
               YS=(YY(E(I,M))+YY(E(I,N)))/2.0
               NEW=1
               DO 54 K=1,NN
                  IF(XS.EQ.XX(TN+K-1).AND.YS.EQ.YY(TN+K-1)) THEN D
                     NEW=0
                     E(I,NC)=TN+K-1
                  END IF
 54            CONTINUE
               IF(NEW .EQ. 1) THEN DO
                  XX(TN+NN)=XS
                  YY(TN+NN)=YS
                  E(I,NC)=TN+NN
                  NN=NN+1
               END IF
 53         CONTINUE
 52      CONTINUE
 51   CONTINUE
      TN=TN+NN-1
C     PRINT ,TN
C     PRINT 7744,(I,(E(I,N),N=1,6),I=1,TE)
 7744 FORMAT('0',I4,10X,6I5)
      DO 102 I=1,TN
         YY(I)=YY(I)-200.0
 102  CONTINUE
C     ALTER COORDINATES OF THE GENERATED NODES
      IF(TALT .NE. 0) THEN DO
      DO 55 I=1,TALT
         READ,M,N,X,Y
C        PRINT 305,M,N,X,Y
 305  FORMAT('0',11X,2I6,2F15.8)
         XX(E(M,3+N))=X
         YY(E(M,3+N))=Y
 55   CONTINUE
      END IF
      CON=199.9998437
      DO 401 I=1,TN
```

```
            RN=XX(I)/(CON+YY(I))
            DR=XX(I)/(CON-YY(I))
            IF(YY(I).GT.CON) THEN DO
              ETAA=PI+ATAN(RN)+ATAN(DR)
            ELSE DO
              ETAA=ATAN(RN)+ATAN(DR)
            END IF
            AITA(I)=ETAA
C           PRINT ,I,ETAA
 401      CONTINUE
          PRINT 4477,(I,AITA(I),XX(I),YY(I),I=1,TN)
 4477     FORMAT('0',I4,10X,3F15.4)
          N=TDN-TAD
C         READ IN DIRICHLET VALUES
          READ,(DN(I),DV(I),I=1,N)
C         PRINT 306,(DN(I),DV(I),I=1,N)
 306      FORMAT('0',10X,I5,12X,F15.8)
C
          IF(TAD .NE. 0) THEN DO
          DO 56 I=1,TAD
             READ,M,NN,D
C            PRINT 307,M,NN,D
 307      FORMAT('0',11X,2I6,F15.8)
             DN(N+I)=E(M,3+NN)
             DV(N+I)=D
 56       CONTINUE
          END IF
C         GO TO 8881
          READ,(ROV(I),I=1,TN)
          READ(15,7777) (EMTP(I),C2(I),C3(I),RM2(I),RM3(I),I=1,TN)
 7777     FORMAT('0',5F12.3)
          AREA=0.0
C         DEFINE COORDINATES OF GAUSS POINTS AND WEIGHTS
          IF(NGP.EQ.3) THEN DO
             GPX(1)=GPY(2)=0.0
             GPY(1)=GPX(2)=GPX(3)=GPY(3)=0.5
             W(1)=W(2)=W(3)=1.0/6.0
          END IF
          IF(NGP.EQ.9) THEN DO
          GPX(1)=GPX(2)=GPX(3)=0.1127017
          GPX(4)=GPX(5)=GPX(6)=0.5
          GPX(7)=GPX(8)=GPX(9)=0.8872983
          GPY(1)=GPY(9)=0.1
          GPY(2)=GPY(6)=0.4436492
          GPY(4)=GPY(8)=0.0563509
          GPY(3)=0.7872983
          GPY(5)=0.25
          GPY(7)=0.0127017
          W(1)=W(3)=0.0684644
          W(4)=W(6)=0.0617284
          W(7)=W(9)=0.0086961
          W(2)=0.109543
          W(5)=0.0987654
          W(8)=0.0139138
          END IF
```

```
      IF(NGP.EQ.4) THEN DO
         GPX(1)=GPY(1)=1.0/3.0
        GPX(2)=GPY(2)=GPY(3)=GPX(4)=0.2
         GPX(3)=GPY(4)=0.6
         W(1)=-27.0/96.0
         W(2)=W(3)=W(4)=25.0/96.0
      END IF
C
C     DEFINE ENTRIES OF MATRIX J AT GAUSS POINT K
      DO 1 K=1,NGP
         J(K,1,3)=0.0
         J(K,1,5)=-4.0*GPY(K)
         J(K,1,1)=4.0*(GPX(K)+GPY(K))-3.0
         J(K,1,4)=4.0-8.0*GPX(K)-4.0*GPY(K)
         J(K,1,2)=4.0*GPX(K)-1.0
         J(K,1,6)=4.0*GPY(K)
         J(K,2,3)=4.0*GPY(K)-1.0
         J(K,2,5)=4.0-4.0*GPX(K)-8.0*GPY(K)
         J(K,2,1)=4.0*(GPX(K)+GPY(K))-3.0
         J(K,2,4)=-4.0*GPX(K)
         J(K,2,2)=0.0
         J(K,2,6)=4.0*GPX(K)
 1    CONTINUE
C
C     DEFINE VALUES OF SHAPE FUNCTION AT GAUSS POINT K
      DO 2 K=1,NGP
         AGP(K,3)=GPY(K)*(2.0*GPY(K)-1.0)
         AGP(K,5)=4.0*GPY(K)*(1.0-GPX(K)-GPY(K))
         AGP(K,1)=(1.0-GPX(K)-GPY(K))*(1.0-2.0*GPX(K)-2.0*GPY(K))
         AGP(K,4)=4.0*(1.0-GPX(K)-GPY(K))*GPX(K)
         AGP(K,2)=GPX(K)*(2.0*GPX(K)-1.0)
         AGP(K,6)=4.0*GPX(K)*GPY(K)
 2    CONTINUE
C
C     INITIALIZE THE MATRICES A AND S
      LIST(1)=750
      DO 33 I=1,TE
         SUM=0.0
         DO 34 K=1,6
            NU=E(I,K)
            SUM=SUM+ROV(NU)
 34      CONTINUE
         ROU(I)=SUM/6.0
C        PRINT ,I,ROU(I)
 33   CONTINUE
      DO 456 IT=6,7
         KOUNT=1
          DO 1001 ITN=1,KOUNT
              LIST(ITN)=0
 1001      CONTINUE
          DO 43 II=2,3
      DO 8 M=1,TN
         C(M)=0.0
         DO 9 N=1,TN
            S(M,N)=0.0
```

```
 9        CONTINUE
 8     CONTINUE
C
C      MAIN PROGRAM TO ACCUMULATE MATRICES
       DO 3 T=1,TE
          DO 5 U=1,6
             XG(U)=XX(E(T,U))
             YG(U)=YY(E(T,U))
 5        CONTINUE
          IF(IT .EQ. 1) GO TO 1330
             IF(II .EQ. 3)GO TO 1330
                AK=0.0
                 DO 770 MK=1,6
                    NU=E(T,MK)
          NNODE=1
        DO 4455 KI=1,KOUNT
           IF(NU.EQ.LIST(KI)) THEN DO
              NNODE=0
              AK=AK+ROV(NU)
           END IF
 4455   CONTINUE
           IF(NNODE .NE. 0) THEN DO
           IF(C2(NU) .EQ. 0.0) GO TO 1112
C
C
           IF(AITA(NU) .LE. 0.18) THEN DO
           YMN(NU)=2.0*RM2(13)/(RM2(13)+RM3(13))
           EPN(NU)= 8414.28/RM2(1)/EMTP(1)
           YND(NU)=EMTP(NU)/EMTP(13)
           ROV(NU)=0.5*(EMTP(NU)+EMTP(13)*EPN(NU)*YND(NU)**YMN(NU))
           GO TO 771
           END IF
C
C
           IF(AITA(NU) .LE.0.33) THEN DO
           YMN(NU)=2.0*RM2(14)/(RM3(14)+RM2(14))
           EPN(NU)= 8386.040/EMTP(26)/RM2(26)
           YND(NU)= EMTP(NU)/EMTP(14)
           ROV(NU)=0.5*(EMTP(NU)+EMTP(14)*EPN(NU)*YND(NU)**YMN(NU))
           GO TO 771
           END IF
C
C
           IF(AITA(NU) .LE. 0.55) THEN DO
           YMN(NU)=2.0*RM2(39)/(RM2(39)+RM3(39))
           EPN(NU)= 8056.622/EMTP(27)/RM2(27)
           YND(NU)=EMTP(NU)/EMTP(39)
           ROV(NU)=0.5*(EMTP(NU)+EMTP(39)*EPN(NU)*YND(NU)**YMN(NU))
           GO TO 771
           END IF
C
C
           IF(AITA(NU) .LE. 0.8) THEN DO
           YMN(NU)=2.0*RM2(40)/(RM3(40)+RM2(40))
           EPN(NU)= 7058.956/RM2(52)/EMTP(52)
```

```
      YND(NU)=EMTP(NU)/EMTP(40)
      ROV(NU)=0.5*(EMTP(NU)+EMTP(40)*EPN(NU)*YND(NU)**YMN(NU))
      GO TO 771
      END IF
C
C
      IF(AITA(NU) .LE. 1.0) THEN DO
      YMN(NU)=2.0*RM2(65)/(RM3(65)+RM2(65))
      EPN(NU)= 5722.461/EMTP(53)/RM2(53)
      YND(NU)=EMTP(NU)/EMTP(65)
      ROV(NU)=0.5*(EMTP(NU)+EMTP(65)*EPN(NU)*YND(NU)**YMN(NU))
      GO TO 771
      END IF
C
C
      IF(AITA(NU) .LE. 1.2) THEN DO
      YMN(NU)=2.0*RM2(66)/(RM3(66)+RM2(66))
      EPN(NU)=4423.6127/EMTP(78)/RM2(78)
      YND(NU)=EMTP(NU)/EMTP(66)
      ROV(NU)=0.5*(EMTP(NU)+EMTP(66)*EPN(NU)*YND(NU)**YMN(NU))
      GO TO 771
      END IF
      IF(AITA(NU) .LE. 1.45) THEN DO
      YMN(NU)=2.0*RM2(91)/(RM3(91)+RM2(91))
      EPN(NU)=2823.5826/EMTP(79)/RM2(79)
      YND(NU)=EMTP(NU)/EMTP(91)
      ROV(NU)=0.5*(EMTP(NU)+EMTP(91)*EPN(NU)*YND(NU)**YMN(NU))
      GO TO 771
      END IF
C
C
      IF(AITA(NU) .LE. 1.67) THEN DO
      YMN(NU)=2.0*RM2(92)/(RM3(92)+RM2(92))
      EPN(NU)=1882.3884/EMTP(104)/RM2(104)
      YND(NU)=EMTP(NU)/EMTP(92)
      ROV(NU)=0.5*(EMTP(NU)+EMTP(92)*EPN(NU)*YND(NU)**YMN(NU))
      GO TO 771
      END IF
      IF(AITA(NU) .LE. 1.9) THEN DO
      YMN(NU)=2.0*RM2(117)/(RM3(117)+RM2(117))
      EPN(NU)=1129.433/EMTP(105)/RM2(105)
      YND(NU)=EMTP(NU)/EMTP(117)
      ROV(NU)=0.5*(EMTP(NU)+EMTP(117)*EPN(NU)*YND(NU)**YMN(NU)
      GO TO 771
      END IF
      IF(AITA(NU) .LE. 2.15) THEN DO
      YMN(NU)=2.0*RM2(118)/(RM3(118)+RM2(118))
      EPN(NU)= 752.9554/EMTP(130)/RM2(130)
      YND(NU)=EMTP(NU)/EMTP(118)
      ROV(NU)=0.5*(EMTP(NU)+EMTP(118)*EPN(NU)*YND(NU)**YMN(NU)
      GO TO 771
      END IF
C
C
      IF(AITA(NU) .LE. 2.36) THEN DO
```

```
            YMN(NU)=2.0*RM2(143)/(RM3(143)+RM2(143))
            EPN(NU)= 423.537/EMTP(131)/RM2(131)
            YND(NU)=EMTP(NU)/EMTP(143)
            ROV(NU)=0.5*(EMTP(NU)+EMTP(143)*EPN(NU)*YND(NU)**YMN(NU)
            GO TO 771
            END IF
C
C
            IF(AITA(NU) .LE. 2.6) THEN DO
            ROV(144)=0.85*ROV(143)
            IF(NU .EQ. 144) GO TO 771
            YMN(NU)=2.0*RM2(144)/(RM3(144)+RM2(144))
C           EPN(NU)= 1.94424E7/EMTP(61)/RM2(61)
            YND(NU)=EMTP(NU)/ROV(144)
            ROV(NU)=0.5*(EMTP(NU)+ROV(144)*YND(NU)**YMN(NU))
            GO TO 771
            END IF
C
C
            IF(AITA(NU) .LE. 2.8) THEN DO
            ROV(169)=ROV(144)-0.2*ROV(144)*1.75
            IF(NU .EQ. 169) GO TO 771
            YMN(NU)=2.0*RM2(169)/(RM3(169)+RM2(169))
C           EPN(NU)= 1.928E6/EMTP(80)/RM2(80)
            YND(NU)=EMTP(NU)/ROV(169)
            ROV(NU)=0.5*(EMTP(NU)+ROV(169)*YND(NU)**YMN(NU))
            GO TO 771
            END IF
C
C
            IF(AITA(NU) .LE. 2.95) THEN DO
            ROV(170)=ROV(144)-0.2*ROV(144)*2.5
            IF(NU .EQ. 170) GO TO 771
            YMN(NU)=2.0*RM2(170)/(RM3(170)+RM2(170))
C           EPN(NU)= 8.0673E4/RM2(81)/EMTP(81)
            YND(NU)=EMTP(NU)/ROV(170)
            ROV(NU)=0.5*(EMTP(NU)+ROV(170)*YND(NU)**YMN(NU))
            GO TO 771
            END IF
            IF(AITA(NU) .GE. 2.95) THEN DO
            ROV(195)=ROV(144)-0.2*ROV(144)*3.2
            IF(NU .EQ. 195) GO TO 771
            YMN(NU)=2.0*RM2(195)/(RM3(195)+RM2(195))
C           EPN(NU)= 8.0673E4/RM2(81)/EMTP(81)
            YND(NU)=EMTP(NU)/ROV(195)
            ROV(NU)=0.5*(EMTP(NU)+ROV(195)*YND(NU)**YMN(NU))
            GO TO 771
            END IF
C
C
 1112       CONTINUE
C
C
      ROV(1)=8414.276*2.0/(RM3(1)+RM2(1))
      ROV(26)=8386.0402*2.0/(RM3(26)+RM2(26))
```

```
      ROV(27)=8056.622*2.0/(RM3(27)+RM2(27))
      ROV(52)=7058.956*2.0/(RM3(52)+RM2(52))
      ROV(53)=5722.461*2.0/(RM2(53)+RM3(53))
      ROV(78)=4423.6127*2.0/(RM2(78)+RM3(78))
      ROV(79)=2823.583*2.0/(RM2(79)+RM3(79))
      ROV(104)=1882.3884*2.0/(RM2(104)+RM3(104))
      ROV(105)=1129.433*2.0/(RM2(105)+RM3(105))
      ROV(130)=752.9554*2.0/(RM2(130)+RM3(130))
      ROV(131)=846.0/(RM2(131)+RM3(131))
      ROV(156)=620.0/(RM2(156)+RM3(156))
      ROV(157)=375.00/(RM2(157)+RM3(157))
      ROV(183)=350.000/(RM2(183)+RM3(183))
      ROV(196)=8395.452*2.0/(RM2(196)+RM3(196))
      ROV(281)=8235.449*2.0/(RM2(281)+RM3(281))
      ROV(282)=7529.5535*2.0/(RM2(282)+RM3(282))
      ROV(355)=6287.1771*2.0/(RM2(355)+RM3(355))
      ROV(356)=5082.4486*2.0/(RM2(356)+RM3(356))
      ROV(429)=3529.478*2.0/(RM2(429)+RM3(429))
      ROV(430)=2258.866*2.0/(RM2(430)+RM3(430))
      ROV(503)=1458.851*2.0/(RM2(503)+RM3(503))
      ROV(504)=903.5464*2.0/(RM2(504)+RM3(504))
      ROV(577)=1035.31/(RM2(577)+RM3(577))
      ROV(578)=920.0/(RM2(578)+RM3(578))
771       CONTINUE
              AK=AK+ROV(NU)
              KOUNT=KOUNT+1
              LIST(KOUNT)=NU
       END IF
C      PRINT 273,T,NU,AITA(NU),YMN(NU),YND(NU),EPN(NU),EMTP(NU),ROV
 770    CONTINUE
 273    FORMAT(2I4,6F15.5)
        ROU(T)=AK/6.0
1330    CONTINUE
       DO 30 K=1,NGP
          X=Y=0.0
          J11(K)=J22(K)=J21(K)=J12(K)=0.0
          DO 10 I=1,6
          J11(K)=J(K,1,I)*XG(I)+J11(K)
          J12(K)=J(K,1,I)*YG(I)+J12(K)
          J21(K)=J(K,2,I)*XG(I)+J21(K)
          J22(K)=J(K,2,I)*YG(I)+J22(K)
             X=XG(I)*AGP(K,I)+X
             Y=YG(I)*AGP(K,I)+Y
 10       CONTINUE
          IF(II .EQ. 2) THEN DO
             EPS=ROU(T)
             ROH=0.0
          END IF
          IF(II .EQ. 3) THEN DO
             EPS=1.0
             ROH= ROU(T)
          END IF
          EPSI(K)=EPS
          RO(K)=ROH
         DET(K)=J11(K)*J22(K)-J21(K)*J12(K)
```

```
                AREA=AREA+DET(K)*W(K)
              AA(K)=J22(K)*J22(K)
              BB(K)=J12(K)*J12(K)
              CC(K)=J22(K)*J12(K)
              DD(K)=J21(K)*J21(K)
              EE(K)=J11(K)*J11(K)
              FF(K)=J21(K)*J11(K)
30         CONTINUE
              DO 6 M=1,6
                 SUM=0.0
                 DO 73 K=1,NGP
                    SUM=SUM+DET(K)*W(K)*RO(K)*AGP(K,M)
 73              CONTINUE
                 C(E(T,M))=C(E(T,M))-SUM
                 DO 7 N=M,6
                    ES=0.0
                    DO 21 Z=1,NGP
                       ES=ES+EPSI(Z)/DET(Z)*W(Z)*(J(Z,1,M)*J(Z,1,N)*AA(
     *                 J(Z,2,M)*J(Z,1,N)*CC(Z)+J(Z,1,M)*J(Z,1,N)*DD(Z)
     *                  J(Z,2,M)*J(Z,1,N)*FF(Z))
 21                 CONTINUE
                    S(E(T,M),E(T,N))=S(E(T,M),E(T,N))+ES
                    S(E(T,N),E(T,M))=S(E(T,M),E(T,N))
 7               CONTINUE
 6            CONTINUE
 3         CONTINUE
C
           DO 26 I=1,TDN
              NL=DN(I)
              DO 27 K=I,TDN
                 IF(DN(K) .LE. NL) THEN DO
                    NL=DN(K)
                    NUM=K
                 END IF
 27           CONTINUE
                 NA=DN(I)
                 DN(I)=DN(NUM)
                 DI=DV(I)
                 DN(NUM)=NA
                 DV(I)=DV(NUM)
                 DV(NUM)=DI
 26        CONTINUE
C
           DO 11 I=1,TN
              DO 12 K=1,TDN
                 C(I)=-DV(K)*S(I,DN(K))+C(I)
 12           CONTINUE
 11        CONTINUE
C
C
           K2=NM=MN=1
C          IZ=1
           DO 31 I=1,TN
              K1=1
              IF(I.NE.DN(K2)) THEN DO
```

```
            B(MN)=C(I)
            MN=MN+1
            DO 32 M=1,TN
               IF(M.NE.DN(K1)) GO TO 133
                  GO TO 417
133               IF(M.GT.I) GO TO 32
               A(NM)=S(M,I)
           NM=NM+1
            GO TO 32
417          IF (TDN .GE. K1+1) THEN DO
                  K1=K1+1
             END IF
32          CONTINUE
         ELSE DO
            IF (TDN .GE. K2+1) THEN DO
               K2=K2+1
            END IF
         END IF
31    CONTINUE
      N=TN-TDN
C
      MS=1
      DO 1030 JJ=1,N
         DO 1040 I=1,JJ
            S(JJ,I)=A(MS)
            S(I,JJ)=S(JJ,I)
            MS=MS+1
1040     CONTINUE
1030  CONTINUE
      NKI=N*(N+1)/2
      DO 6768 I=1,NKI
6768  A(I)=0.0
C     PRINT,'AREA IS',AREA
      NN=1
      DO 1120 I=1,N
          KOUNT=1
          DO 1130 JJ=1,I
              IF(S(JJ,I).EQ.0.0) GO TO 1130
                 DO 1140 K=JJ,I
                    KP=I+KOUNT-K
                  A(NN)=S(KP,I)
                    IF(KP.EQ.I) THEN DO
                       MAXA(I)=NN
C                      PRINT ,I,MAXA(I)
                    END IF
                    NN=NN+1
1140             CONTINUE
                GO TO 1120
1130       KOUNT=KOUNT+1
1120  CONTINUE
      MAXA(672)=NN
      NNK=NN-1
C
C
      N=TN-TDN
```

```
      NWA=N+1
      NN=NNK
      KKK=1
      CALL COLSOL
      KKK=2
      CALL COLSOL
C
C
C
C     REORGANZE NODE NUMBERINGS FOR OUTPUT
      K=1
      M=0
      DO 20 I=1,TN
         IF (I .NE. DN(K)) THEN DO
            M=M+1
            C(I)=B(M)
         ELSE DO
            C(DN(K))=DV(K)
            IF (TDN .GE. K+1) THEN DO
               K=K+1
            END IF
         END IF
         IF(II .EQ. 2) THEN DO
            C2(I)=C(I)
         END IF
         IF(II .EQ. 3) THEN DO
            C3(I)=C(I)
         END IF
 20    CONTINUE
C
C     CALCULATES THE VALUE OF THE FUNCTIONAL
      F=0.0
      DO 24 M=1,TN
         DO 25 I=1,TN
            F=F+S(M,I)*C(I)*C(M)
 25      CONTINUE
 24    CONTINUE
C        PRINT 1155,IT,F
 1155 FORMAT(10X,I6,F15.8)
C
C     PRINT 101
C    PRINT 200,(I,(E(I,N),N=1,6),I=1,TE)
 200  FORMAT('0',10X,I8,10X,6I5)
C     PRINT 101
C     PRINT 100,(I,XX(I),YY(I),I=1,TN)
      DO 1600 K=1,TE
      X1=XX(E(K,1))
      X2=XX(E(K,2))
      X3=XX(E(K,3))
      X4=XX(E(K,4))
      X5=XX(E(K,6))
      X6=XX(E(K,5))
      Y1=YY(E(K,1))
      Y2=YY(E(K,2))
      Y3=YY(E(K,3))
```

```
      Y4=YY(E(K,4))
      Y5=YY(E(K,6))
      Y6=YY(E(K,5))
      V1=C(E(K,1))
      V2=C(E(K,2))
      V3=C(E(K,3))
      V4=C(E(K,4))
      V5=C(E(K,6))
      V6=C(E(K,5))
      O(1,1)=X1*X1-X2*X2
      O(2,1)=X2*X2-X3*X3
      O(3,1)=X3*X3-X4*X4
      O(4,1)=X4*X4-X5*X5
      O(5,1)=X5*X5-X6*X6
      O(1,2)=Y1*Y1-Y2*Y2
      O(2,2)=Y2*Y2-Y3*Y3
      O(3,2)=Y3*Y3-Y4*Y4
      O(4,2)=Y4*Y4-Y5*Y5
      O(5,2)=Y5*Y5-Y6*Y6
      O(1,3)=X1*Y1-X2*Y2
      O(2,3)=X2*Y2-X3*Y3
      O(3,3)=X3*Y3-X4*Y4
      O(4,3)=X4*Y4-X5*Y5
      O(5,3)=X5*Y5-X6*Y6
      O(1,4)=X1-X2
      O(2,4)=X2-X3
      O(3,4)=X3-X4
      O(4,4)=X4-X5
      O(5,4)=X5-X6
      O(1,5)=Y1-Y2
      O(2,5)=Y2-Y3
      O(3,5)=Y3-Y4
      O(4,5)=Y4-Y5
      O(5,5)=Y5-Y6
      R(1)=V1-V2
      R(2)=V2-V3
      R(3)=V3-V4
      R(4)=V4-V5
      R(5)=V5-V6
      IA=5
      N=5
      MA=5
      IB=5
      M=1
      IJOB=0
      CALL LEQIF(O,IA,N,MA,R,IB,M,IJOB,WARA,IER)
      U1(K)=R(1)
      U2(K)=R(2)
      U3(K)=R(3)
      U4(K)=R(4)
      U5(K)=R(5)
C     PRINT 1616,U1(K),U2(K),U3(K),U4(K),U5(K)
 1600 CONTINUE
      DO 1609 I=1,TN
         I5=0
```

```
         AN=0.0
         BN=0.0
         DO 1610 N=1,TE
       IF((I.EQ.E(N,1)).OR.(I.EQ.E(N,2)).OR.(I.EQ.E(N,3)).OR.
     *   (I.EQ.E(N,4)).OR.(I.EQ.E(N,5)).OR.(I.EQ.E(N,6)))GO TO 1612
         GO TO 1610
1612     GRADX=-1.0*(2.*U1(N)*XX(I)+U3(N)*YY(I)+U4(N))
         GRADY=-1.0*(2.*U2(N)*YY(I)+U3(N)*XX(I)+U5(N))
         GX(N)=GRADX
         GY(N)=GRADY
         BN=BN+GX(N)
         AN=AN+GY(N)
         I5=I5+1
         AAA=I5
1610      CONTINUE
      FX=BN/AAA
      FY=AN/AAA
            IF (FY) 61,62,63
61             IF (FX) 64,65,66
62             IF (FX) 67,999,68
63             IF (FX) 69,70,71
64                THETA=(PI+ATAN(FY/FX))*180.0/PI
                  GO TO 666
65                THETA=(3.0*PI/2.0)*180.0/PI
                  GO TO 666
66                THETA=(2.0*PI-ATAN(-FY/FX))*180.0/PI
                  GO TO 666
67                THETA=180.0
                  GO TO 666
68                THETA=0.0
                  GO TO 666
69                THETA=(PI-ATAN(-FY/FX))*180.0/PI
                  GO TO 666
70                THETA=90.0
                  GO TO 666
71                THETA=(ATAN(FY/FX))*180.0/PI
                  GO TO 666
999               PRINT 988
666   RM=SQRT(FX**2+FY**2)
      IF(II .EQ. 2) THEN DO
         RM2(I)=RM
         THETA2(I)=THETA
      END IF
      IF(II .EQ. 3) THEN DO
         RM3(I)=RM
         THETA3(I)=THETA
      END IF
      GO TO 667
988   FORMAT(1H,,'ANGLE INDETERMINATE')
667   CONTINUE
1609  CONTINUE
      PRINT 1222,F
1222  FORMAT(10X,E15.8)
43    CONTINUE
      SUM=0.0
```

```
      DO 3113 IM=1,8
         IM1=13*(2*IM-1)
         IM2=IM1+1
         AJ1=1.8*4.427E-14*ROV(IM1)*(RM2(IM1)+RM3(IM1))
         IF(IM .EQ. 8) THEN DO
            AJ2=0.0
         ELSE DO
            AJ2=1.8*4.427E-14*ROV(IM2)*(RM2(IM2)+RM3(IM2))
         END IF
      SUM=SUM+AJ1+AJ2
3113  CONTINUE
      SUMI=SUM*PI*1.0E8/30.0
      EXPT=38.95
      ERRI=(SUMI-EXPT)*100.0/EXPT
      PRINT 123,IT,SUMI,EXPT,ERRI,ALPHA
123   FORMAT(' ',12X,'ITERATION # =',I6//12X,
     1         'I-TOTAL =',F9.3//12X,
     2         'I-EXPTL =',F9.3//12X,
     3         'ERROR-I =',F9.3//12X,
     4         'ALPHA =',F4.1//12X,
     5         'BEETA =',F4.1/'I')
        PRINT 1000
1000  FORMAT(128('-')//'NODE #',3X,'PHIA',7X,'PHIB',
     *5X,'ERROR-PHY',4X,'EA',8X,'EB',6X,'ERROR-E',
     *2X,'RHO-NEW',3X,'RHO-OLD',3X,'ERROR-RHO',
     *4X,'JA',8X,'JB',6X,'ERROR-J'//128('-'))
      DO 1234 JL=1,TN
      ERRE=(RM3(JL)-RM2(JL))*200.0/((RM3(JL)+RM2(JL)))
      PP(JL)=ROV(JL)*8.854E-14
      IF(IT .EQ. 1) GO TO 2666
      DP(JL)=EMTP(JL)*8.854E-14
2666  CONTINUE
      IF(IT .EQ. 1) GO TO 5555
      IF ((ROV(JL) .EQ. 0.0) .OR. (EMTP(JL) .EQ. 0.0)) THEN DO
          ERRR=0.0
      ELSE DO
      ERRR=(ROV(JL)-EMTP(JL))*100.0/EMTP(JL)
      END IF
      GO TO 5556
5555  ERRR=0.0
      EMTP(JL)=ROV(JL)
5556  CONTINUE
      AJ=1.8*ROV(JL)*8.854E-04*RM3(JL)
      BJ=1.8*ROV(JL)*8.854E-04*RM2(JL)
      IF(AJ .EQ. 0.0) THEN DO
        ERRJ=0.0
      ELSE DO
      ERRJ=(AJ-BJ)*200.0/(AJ+BJ)
      END IF
      IF(C2(JL) .EQ .0.0) THEN DO
        ERRP=0.0
      ELSE DO
        ERRP=(C3(JL)-C2(JL))*200.0/(C2(JL)+C3(JL))
      END IF
      PRINT 2233,JL,C3(JL),C2(JL),ERRP,RM3(JL),RM2(JL),ERRE,PP(JL)
```

```
     1DP(JL),ERRR,AJ,BJ,ERRJ
 1234  CONTINUE
 2233  FORMAT('0',I3,2F11.3,F8.3,2E11.4,F10.3,2E11.4,F10.3,2E11.4,F
       IF(IT .NE. 1) THEN DO
       PRINT 6333,(IN,EMTP(IN),YMN(IN),YND(IN),EPN(IN),
     1 ROV(IN),IN=1,TN)
 6333  FORMAT('0',I4,5F15.8)
       END IF
       DO 332 I=1,TN
 332   EMTP(I)=ROV(I)
 456   CONTINUE
C      PRINT 100,(I,C(I),XX(I),YY(I) ,I=1,TN)
 100   FORMAT('0',10X,I8,10X,3F10.5/)
C100   FORMAT('0',10X,I8,10X,F10.5,10X,1X,F10.5,6X,F10.5/)
C      WRITE(15,7778) (EMTP(I),C2(I),C3(I),RM2(I),RM3(I),I=1,TN)
 7778  FORMAT('0',5F12.3)
 8881  CONTINUE
       STOP
       END
C
C
       SUBROUTINE COLSOL
C
C . . . . . . . . . . . . . . . . . . . . . . . . . . . . . . . .
C .
C .   P R O G R A M
C .      . TO SOLVE SIMULTANEOUS EQUATIONS IN CORE, USING COMPACTED
C .        STORAGE AND COLUMN REDUCTION SCHEME
C .
C .        A    = MATRIX STORED IN COMPACTED FORM
C .        V    = VECTOR TO BE REDUCED
C .        MAXA = VECTOR CONTAINING ADDRESSES OF DIAGONAL ELEMENTS
C .                 OF A
C .        NN   = NUMBER OF EQUATIONS
C .        NWK  = NUMBER OF ELEMENTS BELOW SKYLINE OF MATRIX A
C .        NNM  = NN+1
C .        KKK  = INPUT FLAG
C .        IOUT = NUMBER OF OUTPUT DEVICE
C .
C . . . . . . . . . . . . . . . . . . . . . . . . . . . . . . . .
C
       COMMON/VENKA/A(230000),V(750),MAXA(700),NN,NWK,NNM,KKK
       IF (KKK-2) 40,150,150
 40    DO 140 N=1,NN
       KN=MAXA(N)
       KL=KN+1
       KU=MAXA(N+1)-1
       KH=KU-KL
       IF (KH) 110,90,50
 50    K=N-KH
       IC=0
       KLT=KU
       DO 80 J=1,KH
       IC=IC+1
       KLT=KLT-1
```

```
      KI=MAXA(K)
      ND=MAXA(K+1)-KI-1
      IF (ND) 80,80,60
 60   KK=MIN0(IC,ND)
      C=0.0
      DO 70 L=1,KK
 70   C=C+A(KI+L)*A(KLT+L)
      A(KLT)=A(KLT)-C
 80   K=K+1
 90   K=N
      B=0.0
      DO 100 KK=KL,KU
      K=K-1
      KI=MAXA(K)
      C=A(KK)/A(KI)
      B=B+C*A(KK)
 100  A(KK)=C
      A(KN)=A(KN)-B
 110  IF (A(KN)) 120,120,140
 120  WRITE(6,2000) N,A(KN)
      STOP
 140  CONTINUE
      RETURN
C     REDUCE THE LOAD VECTOR
 150  DO 180 N=1,NN
      KL=MAXA(N)+1
      KU=MAXA(N+1)-1
      IF (KU-KL) 180,160,160
 160  K=N
      C=0.0
      DO 170 KK=KL,KU
      K=K-1
      C=C+A(KK)*V(K)
 170  CONTINUE
      V(N)=V(N)-C
 180  CONTINUE
C     BACK SUBSTITUTE
      DO 200 N=1,NN
      K=MAXA(N)
      V(N)=V(N)/A(K)
 200  CONTINUE
 714  FORMAT(2I8,E12.5)
      IF (NN .EQ. 1) RETURN
      N=NN
      DO 230 L=2,NN
      KL=MAXA(N)+1
      KU=MAXA(N+1)-1
      IF(KU-KL) 230,210,210
 210  K=N
      DO 220 KK=KL,KU
      K=K-1
      V(K)=V(K)-A(KK)*V(N)
 220  CONTINUE
 711   FORMAT(2X,I8,3E15.8)
 230  N=N-1
```

```
      RETURN
2000  FORMAT(//48H STOP-STIFFNESS MATRIX NOT POSITIVE DEFINITE  ,/,
     1          32H NON POSITIVE PIVOT FOR EQUATION  ,I4,//
     2          10H PIVOT =  ,E20.12)
      END
101   FORMAT('1')
     ENTRY
```

DATA INPUT FOR FEP (2-D)

1) TE = Total number of elements
   TN = Total number of nodes at input
   TDN = Total number of Dirichlet nodes (including secondary nodes that are Dirichlet)
   TALT = Total number of altered secondary nodes
   TAD = Total number of secondary nodes that are Dirichlet nodes
   NGP = Number of Gauss point quadrature

2) Major nodes of triangular elements ex: 1 2 3

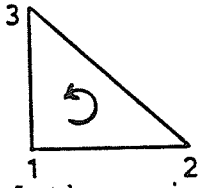

3) (x,y) coordinates of the major nodes

4) Altered coordinates of the secondary nodes
   ex: 3 2 x y
   element# arm# new coordinates

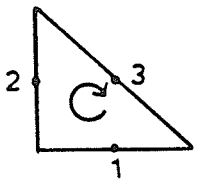

5) Major Dirichlet nodes
   ex: 2 100.0
   node# Dirichlet value

6) Secondary Dirichlet nodes
   ex: 3 2 100.0
   element# arm# Dirichlet value

Appendix C

MESH GENERATING PROGRAM

```
//VENKA JOB '0817124,,,T=5,L=5,C=1,I=20','VENKA'
//   EXEC FORTXCLG,USERLIB='SYS4.EPIC.LINK'
//FORT.SYSIN DD *
C.....................................................................
C
C
C        NELM: TOTAL # OF ELEMENTS.
C        NNOD: TOTAL # OF PRINCIPAL NODES.
C        DND(I,J) CORRESPOND TO X,Y COORDINATES.
C        NELM: TOTAL # OF ELEMENTS.
C        NNOD: TOTAL # OF PRINCIPAL NODES.
C        DND(I,J) CORRESPOND TO X,Y COORDINATES.
C
C
C.....................................................................
        DIMENSION IBUF(4000),NEL(1000,3),DND(1000,3)
        READ(5,*)NELM,NNOD
       WRITE(6,100)NELM,NNOD
 100    FORMAT(20X,'THE NO. OF ELEMENTS',I3,2X,'THE NO. OF NODES',I3
        DO 5 I=1,NELM
        READ(5,*)(NEL(I,J),J=1,3)
 5      WRITE(6,97)(NEL(I,J),J=1,3)
 97     FORMAT('0',20X,3I4)
        DO 6 I=1,NNOD
        READ(5,*)(DND(I,J),J=1,2)
 6      WRITE(6,98)(DND(I,J),J=1,2)
 98     FORMAT('0',10X,2F15.4)
C       PICK MAX. AND MIN. X AND Y
C       SELECT THE LARGEST DIFFERENCE OF X AND Y
        A=0.0
        B=0.0
        A1=0.0
        B1=0.0
        DO 7 I=1,NNOD
        IF(DND(I,1).GE.A)A=DND(I,1)
        IF(DND(I,1).LT.A1)A1=DND(I,1)
        IF(DND(I,2).GE.B)B=DND(I,2)
        IF(DND(I,2).LT.B1)B1=DND(I,2)
 7      CONTINUE
        G=B
        IF(A.GE.B)G=A
        IF(G.GT.6.0)GO TO 10
        S=6.0/G
        GO TO 11
 10     S=6.0/G
```

```
11      DO 12 I=1,NNOD
        DO 12 J=1,2
12      DND(I,J)=DND(I,J)*S
        CALL PLOTS(IBUF,4000)
        CALL PLOT(1.0,6.0,-3)
        DO 14 I=1,NELM
        N1=NEL(I,1)
        N2=NEL(I,2)
        N3=NEL(I,3)
        X1=DND(N1,1)
        X2=DND(N2,1)
        X3=DND(N3,1)
        Y1=DND(N1,2)
        Y2=DND(N2,2)
        Y3=DND(N3,2)
        CALL PLOT(X1,Y1,3)
        CALL PLOT(X2,Y2,2)
        CALL PLOT(X3,Y3,2)
        CALL PLOT(X1,Y1,2)
14      CONTINUE
        CALL PLOT(12,0.0,999)
        STOP
        END
/*
//GO.SYSIN DD *
```

Appendix D

MATRIX ELEMENTS STORAGE

A very important aspect in the computer implementation of any method for solving system of algebraic equations is that a minimum time should be used. In addition, high-speed storage requirements should be as small as possible to avoid the use of back up storage. An advantage of finite element analysis is that the stiffness matrix is not only symmetric and positive definite but is also banded. The fact that in finite element analysis all non-zero elements are clustered around the diagonal of the system matrices greatly reduces the total number of operations and the storage required in the equation solution. However, this property depends on the nodal point numbering of the mesh, and care must be exercised to obtain an effective nodal point numbering. The Figure D.1 shows the element pattern of a typical stiffness matrix. Derivation of the storage scheme and addressing procedure that is being adopted is as follows. Since the matrix is symmetric, we need to store only elements above and including the diagonal. It can be observed that the elements (i,j) of K(ie. Kij) are zero for $j>i+m$. The value m is known as the half-band width of the matrix. Defining by m the row number of the first nonzero element in column i, the variables m_i , i=1,2...n define the skyline of the ma-

trix, and the variables $(i-m_i)$ are the column heights. Furthermore, the half-band width of the stiffness matrix, m_i, equals the maximum degree of freedom pertaining to any one of the finite elements in the mesh. The column heights vary with i, and it is important that all zero elements are out side the skyline not to be included in equation solution. On the other hand, zero elements within the skyline of the matrix are stored and operated upon, since they will become, in many cases nonzero elements during the matrix reduction. With the column height of the stiffness matrix defined, all elements below the skyline of K can be stored as a one dimensional array; ie the active columns of K including the diagonal elements are stored in A. Figure D-2 shows which storage locations the elements of the matrix K given in the Figure would take in A. The addresses of the diagonal elements of K in A is stored in an array MAXA; ie., the address of the i th diagonal element of K, Kii in A is MAXA(I). From Figure D-2 it can be clearly seen that MAXA(I) is equal to the sum of the column heights upto (i-1)st column plus I. Hence the number of nonzero elements in the i th column of K is equal to MAXA(I+1)-MAXA(I), and the element addresses are MAXA(I),MAXA(I)+1 ... MAXA(I+1)-1.

The storage scheme described above is used in computer program, in Appendix A. The effectiveness of the scheme lies essentially in that no elements outside the skyline are stored and processed in the calculations. It should be borne in mind that in the discussion of the above storage

scheme, it was implicitly assumed that the entire array A does fit into available high speed storage of the computer. Program COLSOL is an active column solver to obtain obtain LDL^T factorization of a stiffness matrix or reduce and back substitute. The complete process gives the solution of the finite element equations. The argument variables and use of the subroutine are defined by means of the comment cards in the program.

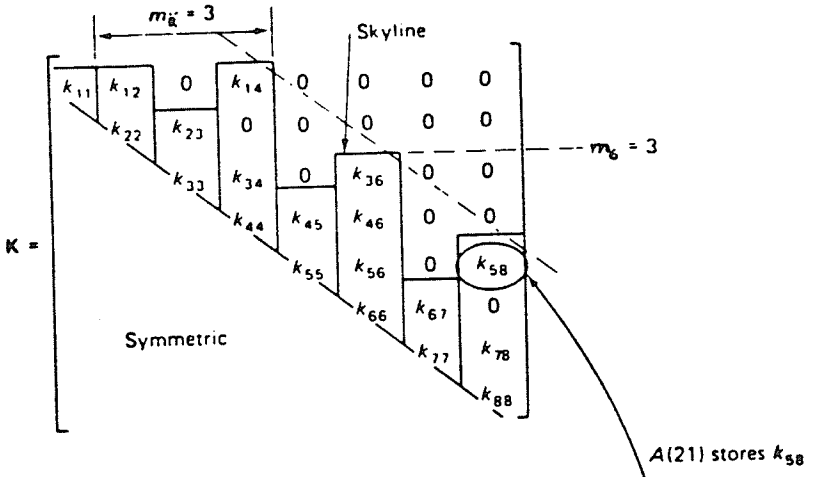

Figure D.1 Actual stiffness matrix

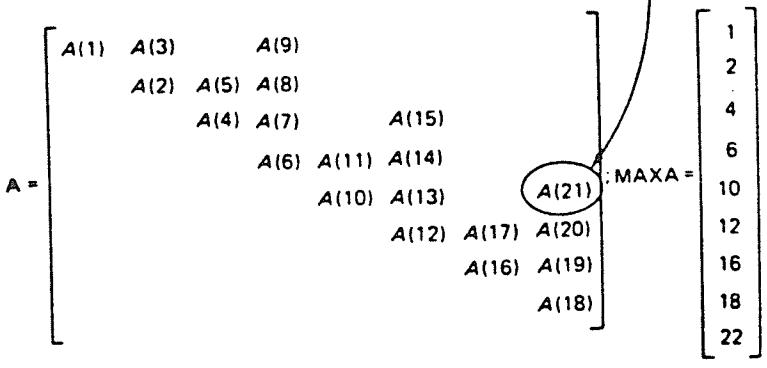

Figure D.2 Storage scheme used for a typical stiffness matrix